THE PERFORMANCE OF A STREAMLINED CROSS-SECTION HEAT PIPE

THE PERFORMANCE OF A STREAMLINED CROSS-SECTION HEAT PIPE

by

SAID HANY MOUSTAPHA, B.Sc.(ENG.)

A Thesis

Submitted to the Faculty of Graduate Studies

in Partial Fulfilment of the Requirements

for the Degree

Master of Engineering

McMaster University

March 1974

MASTER OF ENGINEERING (1974) McMASTER UNIVERSITY
(Mechanical Engineering) Hamilton, Ontario

TITLE: "The Performance of a Streamlined Cross-Section Heat Pipe"

AUTHOR: Said Hany Moustapha, B.Sc. (University of Cairo)

SUPERVISOR: Dr. J. H. T. Wade

NUMBER OF PAGES: xii, 105

SCOPE AND CONTENTS

A streamlined cross-section heat pipe manufactured from 4130 steel, using water as the working fluid and layers of 200 mesh stainless-steel screen for a wick was designed and tested. The experimental effort was directed toward two main objectives. The first objective was to determine the operational details of building a streamlined heat pipe system for experimental use. The second objective was to test the heat pipe at different inclinations to determine the effect of gravity on heat pipe performance.

The axial temperature distributions, performance data and parameters for the streamlined heat pipe, at various power input and angles of inclination, were presented, analysed and compared with existing theories and previous investigations.

The heat pipe transferred a maximum power of 250 watts while installed horizontally. As the evaporator was raised above the condenser level, the maximum heat

decreased, and at the vertical orientation, no thermal equilibrium was attained, at a power input of 25 watts.

The performance of the heat pipe was also compared with that of a solid conductor having the same shape. The equivalent thermal conductivity and specific output calculated, were found to be approximately four and thirteen times respectively greater, than that of a similar solid pure copper rod.

ACKNOWLEDGEMENTS

The author wishes to express his sincere gratitude and appreciation to his supervisor, Dr. J. H. T. Wade, under whose guidance this research was carried out. His many helpful suggestions and continuous encouragement were invaluable throughout the course of the work.

The author is grateful for the assistance and valuable advice given by Dr. R. L. Judd.

This research was supported financially by the National Research Council of Canada, under grant number A-1585.

TABLE OF CONTENTS

LIST OF FIGURES

LIST OF TABLES

NOMENCLATURE

Symbols	Descriptions	Units
A	Area	ft^2 or in^2
D	Rod diameter	in
g	Gravitational acceleration	ft/sec^2
g'	Gravitational constant (32.174)	lb_m ft/lb_f sec^2
k	Thermal conductivity	BTU/hr ft ^oF
K	Wick permeability	ft^2
L	Length	ft or in
$\dot{m}$	Mass flow rate	lb_m/sec
M'	Mach number	-
M	Number of solid rods distributed circumferentially at a certain axial plane	
N	Number of axial rows	
P	Pressure	inches of Hg or lb_f/in^2
Q'	Axial heat conduction	Watts
Q	Heat rate	Watts
r	Radius	ft or in
R	Rod thermal resistance	ft^2 hr ^oF/BTU
T	Temperature	^oF or ^oC
X	Distance	ft or in
α	Heat pipe inclination with horizontal	degree
β	Heat pipe inclination with vertical	degree
Δ	Increment	-

Symbols	Description	Units
ε	Radius of curvature of the pores in the wick	ft
θ	Apparent contact angle	degree
λ	Latent heat of vaporization	BTU/lb_m
μ	Viscosity	$lb_f\ hr/ft^2$
π	Constant (3.1416)	-
ρ	Density	lb_m/ft^3
σ	Surface tension	lb_f/ft
ϕ	Wick porosity	-

Subscripts	Description
a	Adiabatic
c	Condenser, cold
e	Evaporator
eq	Equivalent
h	Hot
i	Input, inlet and inner
ℓ	Liquid
max	Maximum
o	Output, outlet and outer
t	Total
v	Vapor
w	Wick

CHAPTER I

INTRODUCTION

A heat pipe is a self-acting device, which in its simplest form consists of a closed container which is lined with a liquid saturated wick. Heat added at one end transforms the liquid into vapor, which flows to the cooler end where it condenses and releases the latent heat of evaporation. The liquid returns to the heated end through the wick by capillary action.

Due to ease of manufacturing and assembling, the circular cross-section heat pipe has found several investigations and applications. The purpose of this work was to examine the performance of a new shape of heat pipe: a streamlined cross-section heat pipe.

The main idea behind this particular shape was a result of a discussion regarding a heat transfer problem of current interest to United Aircraft of Canada Ltd. The problem involved an air-to-air heat exchanger design of high integrity. A conduction approach to the problem was done through an optimization study presented in Appendix A. The aim of the study was to determine the minimum number of solid conductors, with different limitations on dimension and conductance, capable of transferring the heat load from the hot to the cold stream. The required conductance was found to be excessively high, a

property not normally found in any solid conductors. A solution to the problem however, may be found by substituting for the solid conductor a heat pipe.

A streamlined cross-section heat pipe was chosen as it provided two main advantages over the circular one, especially for a typical aerodynamic configuration. The streamlined cross-section pipe has a lower drag coefficient when compared to that of a right circular cylinder of the same cross sectional area. This is especially important if the heat pipes were to be installed in external flows, for example the by-pass duct of a turbo-jet engine. Secondly, the overall heat transfer coefficient from a streamlined shape is higher than that of a circular shape.

The first objective of the work done was to determine the operational details of manufacturing a streamlined heat pipe system for experimental use. Examples of the operational details sought were: manufacturing of the heat source and sink, temperature measurements instrumentation, difficulties encountered in wrapping and installing the capillary structure, assembly procedure (cleaning, sealing, loading, etc.). The second objective was to test the performance of the streamlined heat pipe installed at different orientations with the horizontal (evaporator up), in order to determine what effect gravity has on the heat pipe performance. Performance tests consisted mainly of determining the axial temperature distributions along the heat pipe and power outputs, at different power inputs up to the maximum allowable heat transfer. Other measured and

calculated parameters have also been presented, analysed and compared with existing theories and previous investigations.

The experiments demonstrated the highly desirable characteristics of the heat pipe operation, mainly high heat transfer rates with low temperature gradients, and high heat transfer per unit weight.

CHAPTER II

THE HEAT PIPE: PHENOMENOLOGY AND LITERATURE SURVEY

2.1. Description and Types of Heat Pipes

The heat pipe was first discovered in 1964 by Grover and Cotter (1, 2)[#], and it is simply defined as a self-contained heat transfer device utilizing a vaporization-condensation cycle to achieve extremely high effective thermal conductivities. One possible configuration for this device is a long closed tube having a liquid saturated wick lining its inner walls. If one end of the pipe is heated and the other cooled, as shown in Figure 1, the liquid in the wick vaporizes at the heated end and flows to the cooled end where it condenses. Capillary action in the wick returns the condensed vapor to the heated end. Thus, the latent heat of vaporization of the fluid is transferred in the vaporization-condensation cycle, and an extremely low temperature drop along the pipe ensues.

The heat pipe definition entailed no geometric constraints in regard to its structure; and in fact, a large number of heat pipes of many different shapes have been built and tested. Most heat pipes have consisted of a cylindrical container offering a large length to diameter ratio. However

---

Numbers in brackets designate references.

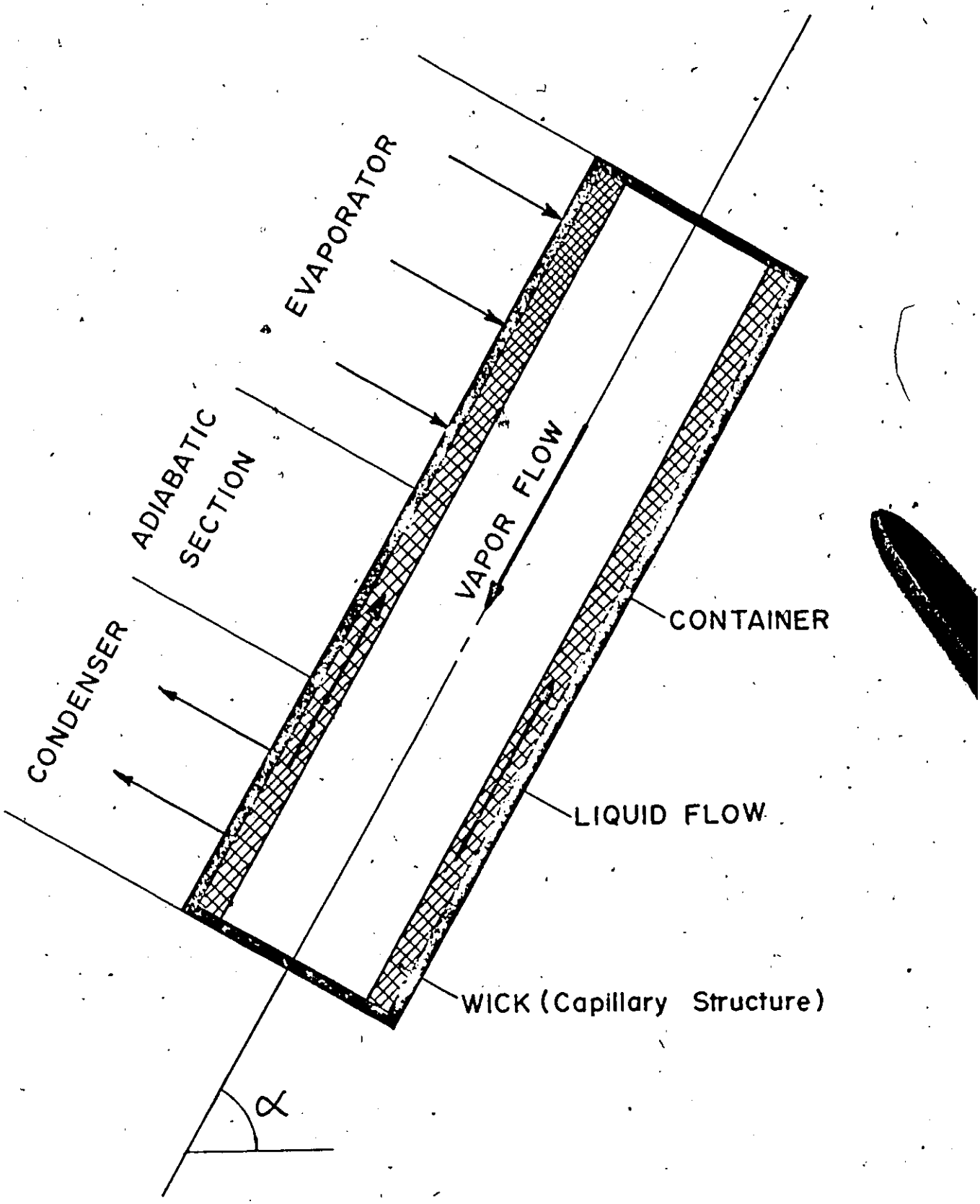

Fig.1 The Heat Pipe

several investigators have proposed and designed radial and flexible heat pipes. A new type of heat pipe that rotated about its longitudinal centerline and utilized centrifugal acceleration instead of capillaries for return-pumping of condensate was presented in 1969 by Gray (3). In 1972, a heat pipe of new design, using an electrode structure to orient and guide the dielectric liquid phase flow was proposed (4).

2.2. Heat Pipe Applications

Theoretically the heat pipe may be applied to almost a limitless number of thermal transport problems, which in general, can be subdivided into four broad topical categories depending on the particular feature of a heat pipe which is to be exploited (5).

The temperature equalizing feature of the heat pipe have prompted numerous suggestions and actual uses for the maintenance of a desired constant temperature environment. As an example, when a spacecraft is subjected to solar radiation the sunny side of the craft approached temperatures of 400°K while the shaded side dropped to about 150°K. A tremendous improvement in uniformity of vehicle temperature was achieved by bonding a series of heat pipes at regular intervals along the vehicle (6).

Heat pipes may also be used to flatten flux variations supplied by an unsteady heat source. Researchers at RCA (7) have developed a heat pipe which maintains a constant thermal output flux independent of variations in thermal input flux

up to a factor of eight or more.

Another use of the heat pipe would allow separation of the heat source from the heat sink. Again, possible spacecraft applications of heat pipes have received considerable attention since the heat source, for instance electronic components, have often been located in the interior of the craft and the waste heat must often be transferred over some distance for ultimate rejection to outer space.

Another feature of the heat pipe, which has generated much enthusiasm, is its ability for thermal flux transformation. Heat addition to and heat removal from a heat pipe were feasible across heat flow areas of different size. This potential for heat flux transformation has stimulated thermionic specialists to consider the conversion of low heat fluxes generated by radioactive isotopes for instance, into a sufficiently high heat flux which is required for the operation of a thermionic converter.

2.3. Material Tests

A very extensive research effort has been devoted to heat pipes since 1964, when Grover and his co-workers (1) at the Los Alamos Scientific Laboratory, first reported the successful operation of a heat pipe. A water heat pipe (30 centimeters long) and two liquid sodium heat pipes (30 centimeters and 90 centimeters long, respectively) were subjected to tests to determine the maximum heat input. Wicking material used was either stainless-steel screen or porous Alundum tubes.

The maximum heat input rate reached was 30 watts per square centimeters of the heated section. It was concluded that this maximum rate was restricted by the deformation or drying of the wick.

Normally the success of operation of any heat pipe depends on the working fluid used, the wicking material and the compatibility of components.

The choice of a working fluid is dictated to a large degree by several physical properties of the fluid and by the chemical compatibility of the fluid with the container and the wick. Deverall and Kemme (8) were the first investigators to formulate the requirements for suitable heat pipe fluids: [1] high latent heat of vaporization, [2] high thermal conductivity, [3] low viscosity, [4] high surface tension, [5] high wetting ability, and [6] a suitable boiling point. Parker and Hanson (9) showed that the vapor pressure curve dictated the temperature range of applicability for a given fluid. The relative merit of various working fluids within a particular temperature range is usually established by comparing the values of a dimensional fluid property group for each fluid. The property group has the dimensions of a heat flux and is defined as the product of the latent heat of vaporization and the surface tension divided by the kinematic viscosity of the fluid($\rho\lambda\sigma/\mu$). Numerous authors have presented plots of the fluid property groups for various fluids as a function of temperature (10, 11, 12, 13). Frank (12) for example has published extensive property group plots for water, sodium,

and cesium, while reference (13) yields values of the property group for liquid metals for possible heat pipe application. Langston and Kunz (14) presented a table comparing the value of the fluid property group for several low temperature fluids including the freons, alcohols, and glycols. Usually liquid metals have been employed in high temperature studies, and common liquids, such as water or the alcohols for low and moderate temperatures. In the intermediate temperature range from 200 to 300°C Deverall (15) has suggested the use of mercury to which a small amount of titanium and manganese has been added to improve the wetting characteristics. Recently Tien (16, 17) and Feldman (18) have predicted the theory and operation characteristics of a two component heat pipe using water combined with different percentages of ethanol (or methanol).

The primary requisite for a heat pipe wick is that it acts as an effective capillary pump, that is, the surface tension forces developed between the fluid and the wick structure must be sufficient to overcome all viscous and gravitational forces, and still maintain the required fluid circulation. The property data on wicking materials which have been accumulated to date, originate primarily from wicking height and permeability measurements.

A wick property of major importance is the maximum height to which a wick lifts a given working fluid. Ferrell and his co-workers (19) measured the equilibrium height of water in packed beds consisting of stainless-steel particles (40 and 100 mesh) and glass beads (80 and 100 mesh). Phillips

and Hinderman (20) measured the maximum capillary pressure for a 200 mesh screen of stainless-steel, bronze, and nickel using water, methanol and benzene, respectively. Reference (21) presented measuremonts of capillary equilibrium levels as functions of particle diameter for packed beds of monel beads. Katzoff (22) measured the lift capability of six screens and found the values of the minimum effective meniscus radius ranging between 0.75 and 0.90 times the spacing of the wires in the screen. McKinney (23) presented a plot between the capillary rise and screen mesh for stainless-steel screen.

The second property of great importance when selecting a wick is its permeability which is defined as a proportionality constant between the flow rate and the pressure drop in a porous body. Reference (21) presented permeability measurements as a function of particle diameter for packed beds of monel beads. Wick permeability for 50, 100 and 200 mesh stainless steel and 100 mesh copper were determined by Roberts and Feldman (24). McKinney (23) presented an experimental determination of permeability for 100 and 250 mesh stainless-steel screens; the results were approximately constant irrespective of flow rate. Langston and Kunz (14) experimentally determined the permeabilities for a number of sintered metallic materials fabricated from felted fibers, powders, and screens. The permeability was found to be independent of the nature of the fluid, time, flow rate and fluid temperature.

A wide variety of wicks have been successfully employed in heat pipes. The most widely used to date, consisted

of several layers of fine mesh screen. Various methods have been used to guarantee mechanical contact between the screen and the container. Neal (11) rolled the screen on a mandrel and upon insertion into the pipe removed the mandrel. The screen was held against the heat pipe wall by its own resilience, but Neal found that the resilience varied from screen to screen and hence the performance of the pipe was not reproducible. Deverall and Kemme (8) forced a steel ball through a heat pipe, after the screen layers have been inserted, and apparently achieved good contact between the wick and the wall. McKinney (23) employed a coiled spring to hold a screen wick firmly against the heat pipe wall. In addition to using screens as wicks, several investigators have employed screens only as a retaining structure. Heat pipes constructed at North Carolina State University (19, 21) have utilized wicks consisting of various types of beads packed in an annulus between a retaining screen and the heat pipe wall. With the exception of screen wicks, the wicking structures which have received the most attention are the so-called low resistance and composite wicks. Bohdansky (25) first suggested the possibility of using channels, cut into the interior surface, running axially along the length of the tube. Kemme (26) advocated the use of composite wicks with a fine pore size at the liquid-vapor interface to provide good capillary pumping and a larger pore size underneath for the return flow of the liquid. Katzoff (22) and Johnson (27) constructed a low resistance wick by forming a single cylindrical passage or artery out of the same sheet of

screen material which covered the interior of the pipe. Ranken and Kemme (28) employed a slotted corrugated stainless-steel sheet which was formed into a cylinder and inserted into a heat pipe. The triangular passages formed between successive corrugations served as low resistance fluid return paths.

2.4. Operating Characteristics of Heat Pipes

In addition to the experiments concerned with basic investigations of potential heat pipe materials, many investigators performed experiments to determine the operating and limiting characteristics of heat pipes.

The heat transport in heat pipes is limited by a number of effects, which can be divided into two groups. The first one stems from liquid flow limitations which is manifested by an interruption of the circulation of the working fluid due to insufficient return flow of liquid, which can be caused by insufficient capillary pressure "wicking limit", or by the formation of bubbles in the wick "boiling limit". These liquid flow limitations can be overcome by suitable design of the wick. The second group stems from vapor flow limitations and presents an ultimate limit of the heat flux in the sense that it cannot be exceeded regardless of wick construction. For these vapor flow limitations, two regimes can be distinguished depending on the relative magnitude of inertia and viscous forces in the vapor. In the inertia flow regime the heat flux is limited by the choking phenomenon or "sonic limit", while in the viscous flow regime the heat flux limitation stems from

the fact that the vapor pressure cannot be smaller than zero, i.e., the "viscous limit".

Neal (11) reported the results of a number of heat pipe experiments using various wick structures. The investigation included an analysis of the heat pipe which resulted in design equations for calculating the maximum heat transferred by the heat pipe at wicking and boiling limit respectively. The analysis also gave a criterion by which working fluids and capillary materials may be chosen. The experimental effort was directed toward two general areas of heat pipe technology. The first one considered factors which determined good capillary structures. Three typos of capillary materials, mainly refrasil, stainless-steel screen and sintered copper fiber were used in heat pipe operation. The second area considered the building and operation of two heat pipe designs to determine their capacities and the mechanism by which they may fail. One pipe was frozen and subjected to a start-up test at a low power level to investigate the possibility of bringing a heat pipe back to life. The heat pipes were operated using both water and ethyl alcohol as working fluids. Conclusions from this report were as follows: [1] The thermal conductivity of nonmetal wicks was too low for their use in heat pipes designed to transfer large heat loads. [2] The power limitations of heat pipes studied were due to a capillary pumping limitation which makes knowledge of the wick pore size and permeability most important for an accurate design of a heat pipe. [3] Start-up of a frozen heat pipe, even at very low power levels, may lead

to a burnout.

Cosgrove (21) presented an analytical model based on the assumption that capillary circulation was the controlling factor in heat pipe operation. The model related the maximum heat input to the fluid and wick characteristics, and to the inclination of the pipe with respect to gravity. It indicated that the critical parameters were the capillary forces in the wick, the pressure drop through the wick, and the operating temperature of the heat pipe. He also investigated two water brass heat pipes in which the wick structures consisted of packed monel beads which were held in an annulus between a retaining screen and the wall. For a particular wick structure and pipe orientation, the maximum heat transfer was considered reached when a hot spot began to form in the evaporator as detected by thermocouples installed in the packed beads. It was concluded that for a given particle diameter, the maximum heat transfer decreased with increasing elevation, and for a selected heat pipe inclination the maximum heat transfer increased with decreasing particle diameter. This effect was caused by the increased capillary pressure resulting from the smaller pore size.

Roberts and Feldman (24) argued that heat pipe theory, assuming a fully saturated wick, has been found to inaccurately predict the heat transfer rate of heat pipes operating at conditions near the burnout heat transfer limit. At conditions near burnout, it has been observed that the liquid level becomes thinner and was supported by the smaller pore radii down in the

wick. This recession of liquid into the wick caused the wick to be only partially saturated and therefore the cross sectional area of wick available for liquid flow was significantly reduced. A theoretical design model has been developed to predict the heat transfer rate for heat pipes operating with partially saturated wicks. This theoretical model was general and could be applied to any type of capillary wick heat pipe once the particular recession distribution was specified. In order to evaluate this recession theory, it was applied to the case of two and three layers screen mesh wicks. Heat transfer rates in water heat pipes with 50, 100 and 200 mesh stainless-steel wicks and 100 mesh copper wick were experimentally measured and were found to agree well with the values predicted by the recession theory.

Marto and Mosteller (29) studied the problem of wick boiling using a so-called everted heat pipe, in which the normal construction of the heat pipe was turned inside out. The unique feature of this pipe was a vapor space enclosed in an annulus between an interior tube and a confining envelope. The wick consisted of four layers of 100 mesh stainless-steel screen attached to the outside of the inner pipe. The outer envelope was made of glass to facilitate visual observation of wick boiling. As the radial heat flux was increased, dryout of the wick occured at the same flux value whether or not boiling was observed. The authors concluded that wick boiling could exist in a heat pipe without having detrimental effect on its operation.

Moss and Kelly (30) employed a neutron radiographic technique to measure the liquid thickness in the wick of the evaporator in a coplanar heat pipe. The wick was made of sintered stainless-steel screen and the working fluid was water. Measurements proved that only under conditions of zero heat transfer did the wick in the evaporator remain completely saturated. As soon as heat was supplied to the evaporator, the liquid interface receded into the wick reducing the extent of saturation in the wick. In addition, the data demonstrated that under normal operating conditions the degree of saturation of the wick in the evaporator was inversely proportional to the heat flux. The authors concluded that a vapor blanket was formed at the base of the wick and that the existence of this blanket manifested itself in the reduced saturation of the wick. Two analytical models were formulated in an attempt to describe the heat transfer characteristics of the partially saturated wick. In a conventional model it was assumed that vaporization takes place at the liquid-vapor interface. In the other model, however, the formation of a vapor blanket at the base of the wick was assumed. For heat fluxes smaller than 15000 BTU/hr $\cdot$ ft^2 the second model more closely predicted the measured values than the more conventional first model.

In a study of the vapor velocity limit in heat pipe operation, Dzakowic (31) employed a sodium-stainless-steel heat pipe with five layers of 60 mesh screen serving as wick. Axial temperature profiles were reported with different rates of heat transport through the pipe. Good correlation was obtained

between the measured and predicted heat transfer limits. A constant ratio of static pressures across the evaporator section was deduced from surface temperature measurements to substantiate the occurrence of sonic velocity.

Busse (32) presented an analysis of the ultimate limit of heat transfer of cylindrical heat pipes with laminar vapor flow, for the two limiting cases of either predominant inertia or viscous forces, taking into consideration both the axial and radial variation of the vapor velocity. The radial variation of the axial velocity was decisive in the viscous flow regime, while in the inertia flow regime its influence turned out to be limited to a 5 percent decrease of the ultimate limit of heat transfer. The vapor was described as an isothermal perfect gas. The analysis showed that for every heat pipe below a certain temperature the ultimate limit of heat transfer was of the viscous type. This limit could be much below the sonic limit. When compared with experimental data, good agreement was found.

Tien (16, 17) measured the axial temperature distribution along the outside of a water-ethanol heat pipe. He determined the pressure inside the pipe and compared this with the pressure which had to prevail if pure ethanol occupied the condenser and pure water occupied the evaporator. He concluded that separation into pure components in a heat pipe was extremely difficult, if not impossible, to achieve. Instead he found that if the initial composition was rich in ethanol, the data attested to the existence of a water-ethanol mixture

in the evaporator while nearly pure ethanol occupied the condenser section.

CHAPTER III

EXPERIMENTAL EQUIPMENT AND PROCEDURES

3.1. General Outline of the Experiments

The apparatus was designed to test the performance of a streamlined cross-section heat pipe. The pipe used was 4130 steel with a wall thickness of 0.029 inch. The cross section of the pipe had a major and a minor axis of 1.35 inches and 0.47 inch respectively. The length of the evaporator, adiabatic and condenser section was respectively 6.0, 0.875 and 2.5 inches. Figure 2 shows the cross-section of the pipe. Also shown, are the thermocouple locations on a schematic plan of the pipe.

Distilled water was used as a working fluid, and the wick consisted of 16 layers of 200 mesh stainless-steel screen lining the interior wall of the pipe.

The heat pipe evaporator section was heated by four cartridge heaters embedded in a brass block, and the condenser section cooled by a water jacket calorimeter.

Figures 3 and 4 show the heat pipe performance test system consisting mainly of the heat pipe apparatus and the three measurement circuits. The input power rate to the heaters was measured by a wattmeter, and the output power rate consisted of measurements of water flow rate by means of a rotameter and temperature difference between the water outlet and inlet

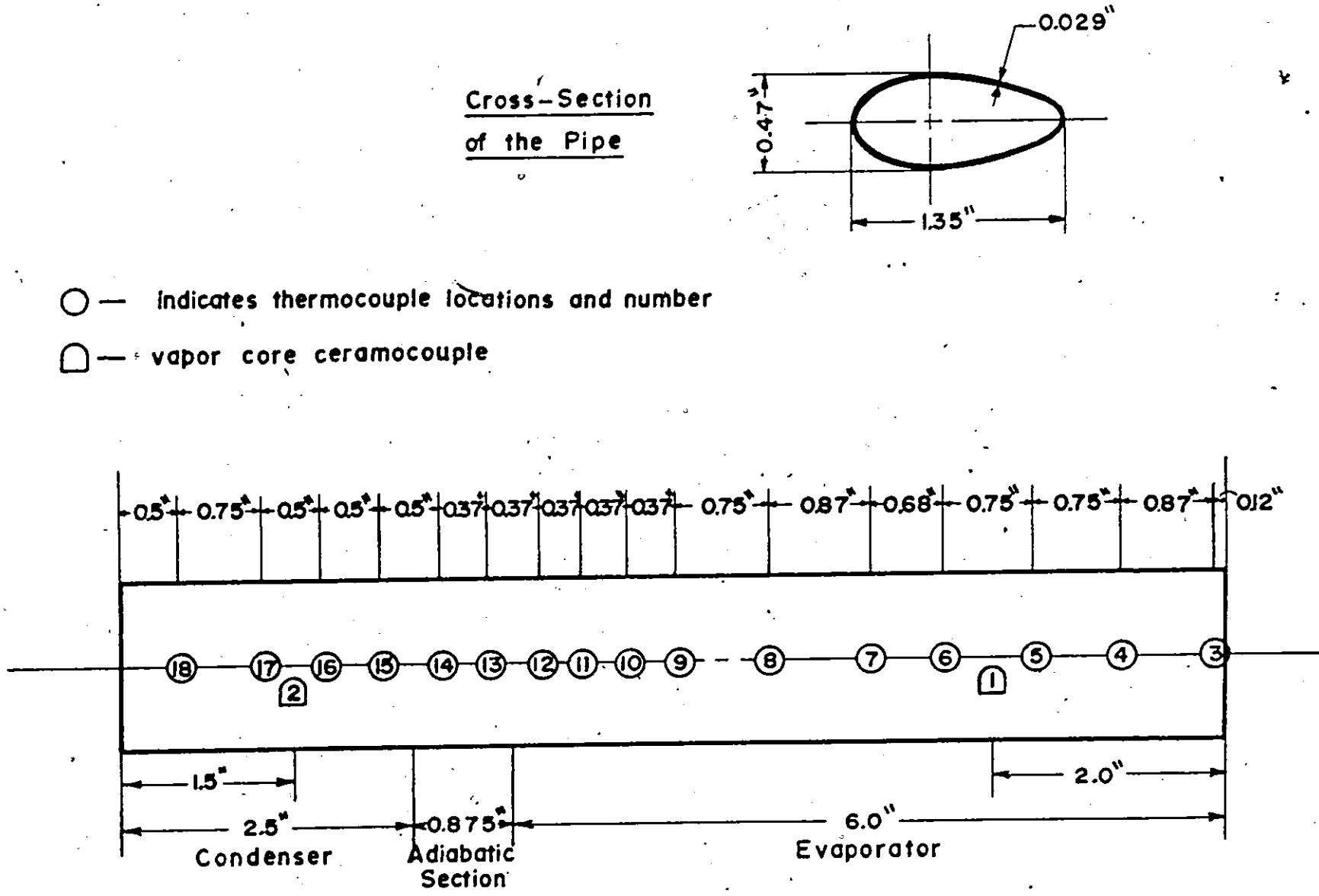

Fig. 2 Thermocouple Locations and Cross-Section of the Pipe

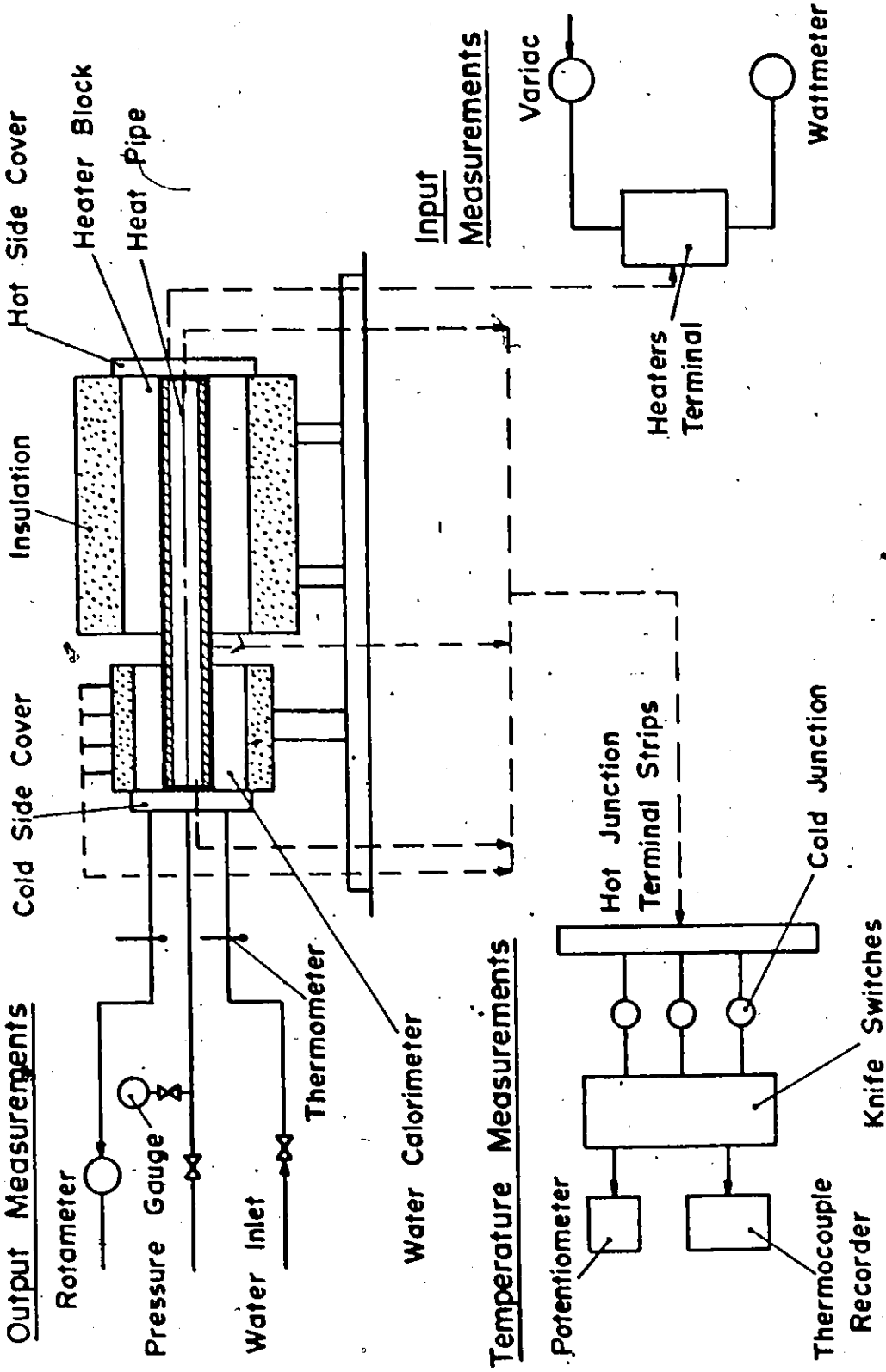

Fig.3 Heat Pipe Performance Test System

CAPTIONS FOR FIGURE 4

A	Wattmeter
B	Heater Terminal Box
C	Variac
D	Evaporator Section
E	Condenser Section
F	Condenser Ceramocouples
G	Vacuum-Fill System
H	Thermometer Wells
I	Hot-Junction Terminal Strips
J	Ice Baths
K	Knife-Switch Board
L	Potentiometer
M	Recorder
N	Rotameter

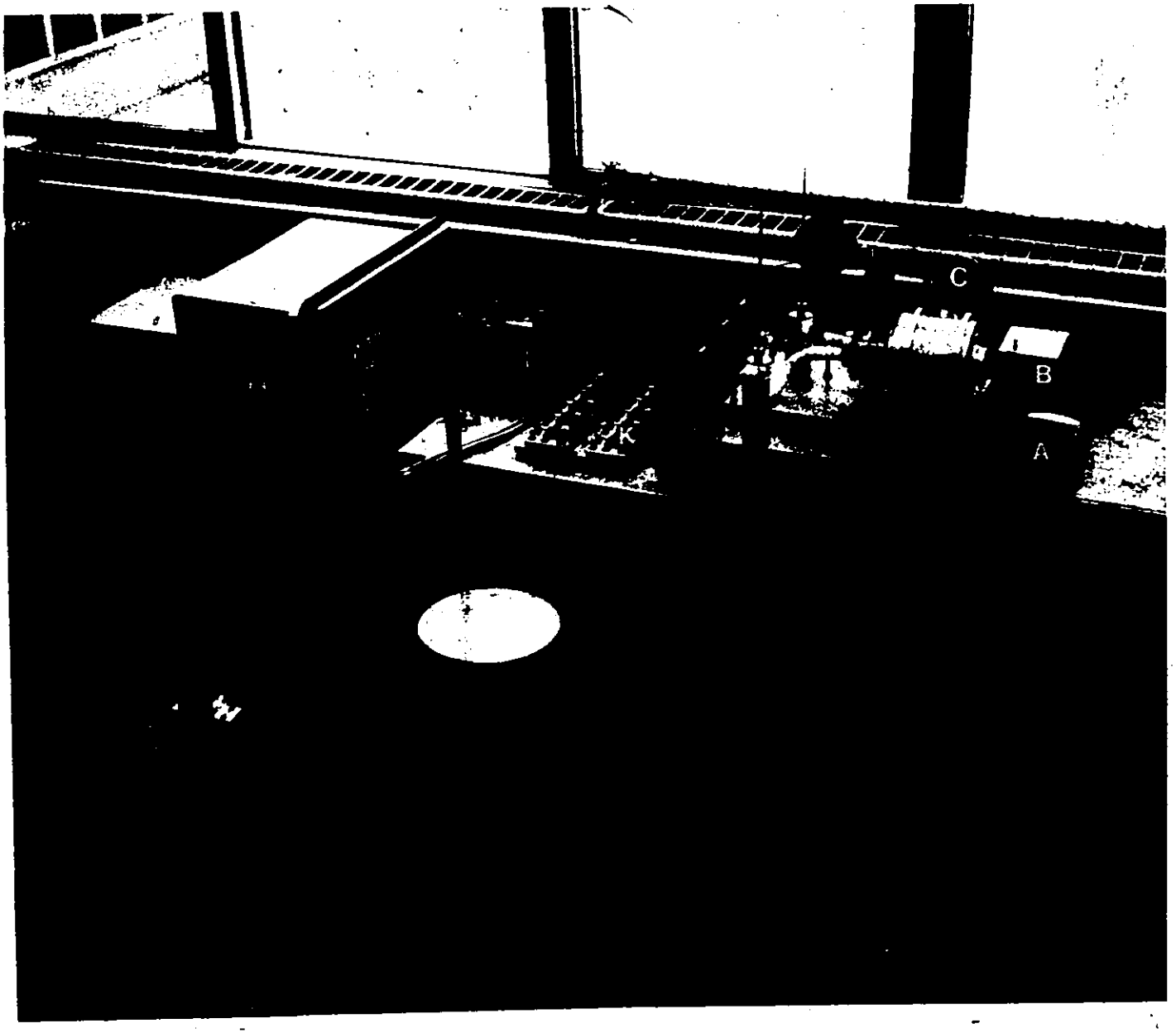

Fig. 4a Experimental Apparatus (Top View)

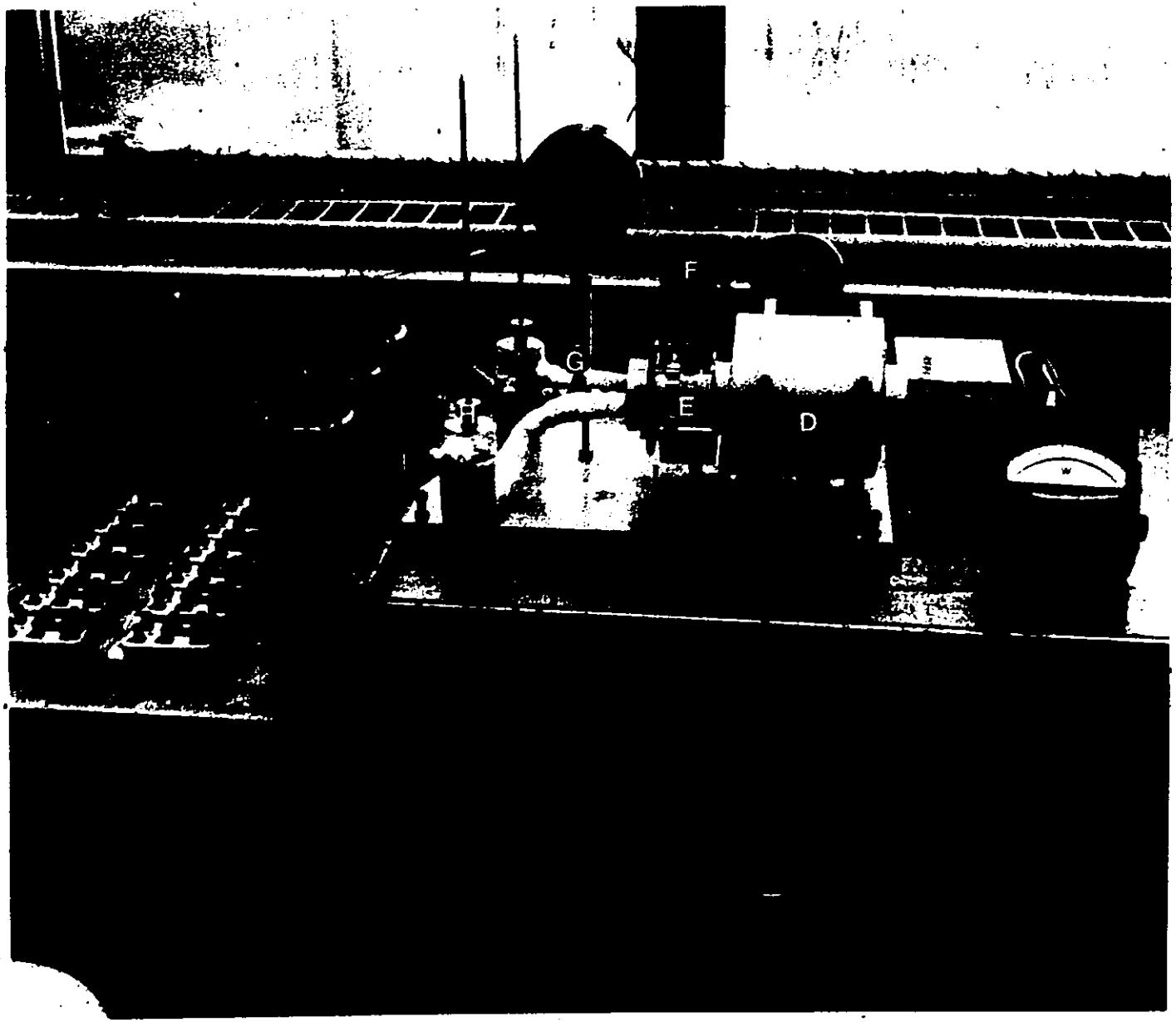

Fig. 4b Experimental Apparatus (Front View)

to the calorimeter. For axial temperature profile measurements, a number of thermocouples were welded at different locations to the outer surface. The temperatures were sequentially recorded by a twelve point recorder. A compound scale pressure gauge (30 inches Hg vacuum to 150 p.s.i.g.) was used to monitor the pressure inside the pipe.

The heat pipe was tested in the horizontal direction, and at an inclination of 15^{o}, 30^{o}, 45^{o} and 90^{o} to the horizontal: the condenser section being down. At each orientation the heaters' power was increased by adjusting the variac, up to the maximum heat that could be transferred by the heat pipe (burn-out condition). For each power level, measurements consisted of the temperature distribution along the heat pipe, the vapor core temperature, the input power, the water mass flow rate, the temperature of the inlet and outlet water to the calorimeter and the pressure inside the heat pipe.

3,2. The Heat Source and Sink

The heat source consisted of four electrical resistance heaters (Chromalox Cartridge Heaters), having each a maximum power of 250 watts, a diameter of 0.375 inch, and a length of 6 inches. The heaters were embedded in a brass annular heater block, 2.5 inches diameter, which was split along its axis and clamped to the outer surface of the heat pipe to provide a good thermal interface and to facilitate assembly and disassembly. The streamlined shape of the heater block's annulus was obtained by means of the Electro-Discharge Machine

(EDM)* using as an electrode a section of the streamlined pipe under consideration. As the stroke of the EDM was less than 6 inches, the heater block was made out of two identical three inch length blocks. Several 0.0625 inch holes were drilled through the top part of the heater block to provide a passage for the thermocouple wires from the heat pipe top surface to the hot junction terminal strips. Heat losses to the atmosphere were minimized by surrounding the heater block with two inches thick fibreglass insulation, eccentric by 0.125 inch with the heater block to provide space for the thermocouple wires. An insulated cover was bolted to the side of the insulation to reduce the axial heat losses. The heat input rate was controlled by a Variac and measured by a watt-meter.

The heat sink consisted of a water jacket calori-meter, 2.5 inches long and 2.75 inches diameter, which was fitted on the condenser section of the heat pipe. Four holes for Swagelock fittings were provided at the calorimeter top for temperature measurements at the heat pipe surface. The calorimeter was surrounded by 1.25 inches thick fibreglass insulation, and an insulated side cover was bolted to the calorimeter end. Heat transfer rates through the heat pipe were determined by measuring the temperature rise and mass flow rate through the water bath. The temperatures entering and leaving the water bath heat sink were measured by mercury-

* ELOX Type TQH 31

in-glass thermometers with a range of -1°C to 51°C having a division of 0.1°C. They were installed in two wells at the entry and the exit of the calorimeter respectively. The thermometer wells and connecting hoses from the calorimeter to the wells were covered with fibreglass insulation. The water rate of flow was measured by a rotameter* placed in the outlet line of the calorimeter.

3.3. Temperature Measurements

Temperature measurements were made with two thermocouple systems. The first consisted of 30 gauge fibreglass insulated chromel-constantan thermocouples. Twelve thermocouples were spot welded at different axial locations (Figure 2) along the upper heat pipe surface on the evaporator and adiabatic section. After the spot welding operation the hot junctions were covered with epoxy for protection. The thermocouple wires were then passed through their respective 0.0625 inch holes in the heater block to the 0.25 inch gap between the heater block and the insulation, and finally to the hot junction terminal strips.

The second system consisted of six iron-constantan, grounded junction, metallic sheathed thermocouples, marketed under the trade name "Ceramocouples". Four ceramocouples with a sheath diameter of 0.125 inch and a length of 4.0 inches were used for recording the axial temperature distribution in the calorimeter (condenser section). Small indentations at the

---

* Brooks Rotameter, Type 8-1307

locations of these ceramocouples were made on the heat pipe surface to ensure a better surface temperature readings. Finally two ceramocouples 0.0625 inch diameter and 6.0 inches long were inserted into the container, one at each end, to a depth of 2.0 inches in the evaporator and 1.5 inches in the condenser. These ceramocouples were designed to measure the vapor core temperature and served two important functions. Of primary importance was the indication of the heat pipe performance status as could be seen by the small vapor temperature difference between both ends of the pipe. The ceramocouple on the condenser side also served along with the pressure gauge reading to compare the experimental vapor pressure with the theoretical one at the corresponding saturation temperature as given by the steam tables.

The cold reference junction consisted of three insulated flasks filled with crushed ice and distilled water. The thermocouples were connected, through the hot junction terminal strips and the flasks, to a twelve knife-switches board (Figures 3 and 4). These switches allowed recording 24 temperature measurements, twelve at a time, on a twelve-point recorder*. The function of the recorder was mainly during the transient period. When steady state was reached the readings were taken by a precision potentiometer** with a division of 0.01 millivolt. Before each test the recorder and the potentiometer were calibrated and readings were made on all

---

* Honeywell Type 15303836.
** Honeywell Type 2745

thermocouples to ensure proper operation.

3.4. Selection and Preparation of the Fluid and the Wick

The choice of a working fluid for a heat pipe application is dictated to a large degree by the physical properties of the fluid and by the chemical compatibility of the fluid with the container and the wick. Probably the first requirement is that the fluid wets the wick material and the pipe. This is necessary because only wetting fluids are pumped by capillary action. Other properties that must be considered also are surface tension, latent heat of vaporization, viscosity, etc.

Due to the availability of distilled water and also for the temperature range dictated by the hot and cold air stream temperatures, (Appendix A), water was used as the working fluid. Water possesses a high latent heat of vaporization, a high surface tension and a wetting ability.

The preparation of water consisted essentially of boiling distilled water for several hours to deoxidize it. Crystals of sodium dichromate were added to the water to reduce the possibility of corrosion of the pipe.

The primary requisite for a heat pipe wick is that it acts as an effective capillary pump. That is, the surface tension forces developed between the fluid and the wick structure must be sufficient to overcome all viscous and other pressure drops in the pipe and still maintain the required fluid

circulation.

The type of wick used in these experiments consisted of several layers of fine mesh screen, which is the most widely used to date. For selecting the mesh type, the capillary rise capability of the wicking material must be determined. For these experiments the capillary rise was 9.5 inches. By observation of Figure 5 taken from reference 23, to obtain a capillary rise of 9.5 inches, the screen should be about 180 mesh. Therefore a 200 mesh stainless-steel screen* with a wire diameter of 0.0021 inch was chosen as the wicking material.

Appendix B outlines the procedure followed for estimating the wick thickness to be used. The screen was cut to the chosen size: 42.25 by 9.375 inches, and then washed with water and acetone.

The rolling of the screen was done by means of a circular wood mandrel 12.0 inches long and 0.75 inch diameter. The diameter of the mandrel was chosen so that the mandrel's perimeter was nearly equal to the inside perimeter of the streamlined pipe after allowing for the wick to line the inner walls of the pipe. The wood mandrel was tappered along its length to facilitate removing it after wrapping the screen. By trial and error, the perimeter of the wood mandrel was reduced so that after wrapping the screen it fitted very closely to the inner wall of the pipe.

---

* Type 304 Greening Donald Ltd.

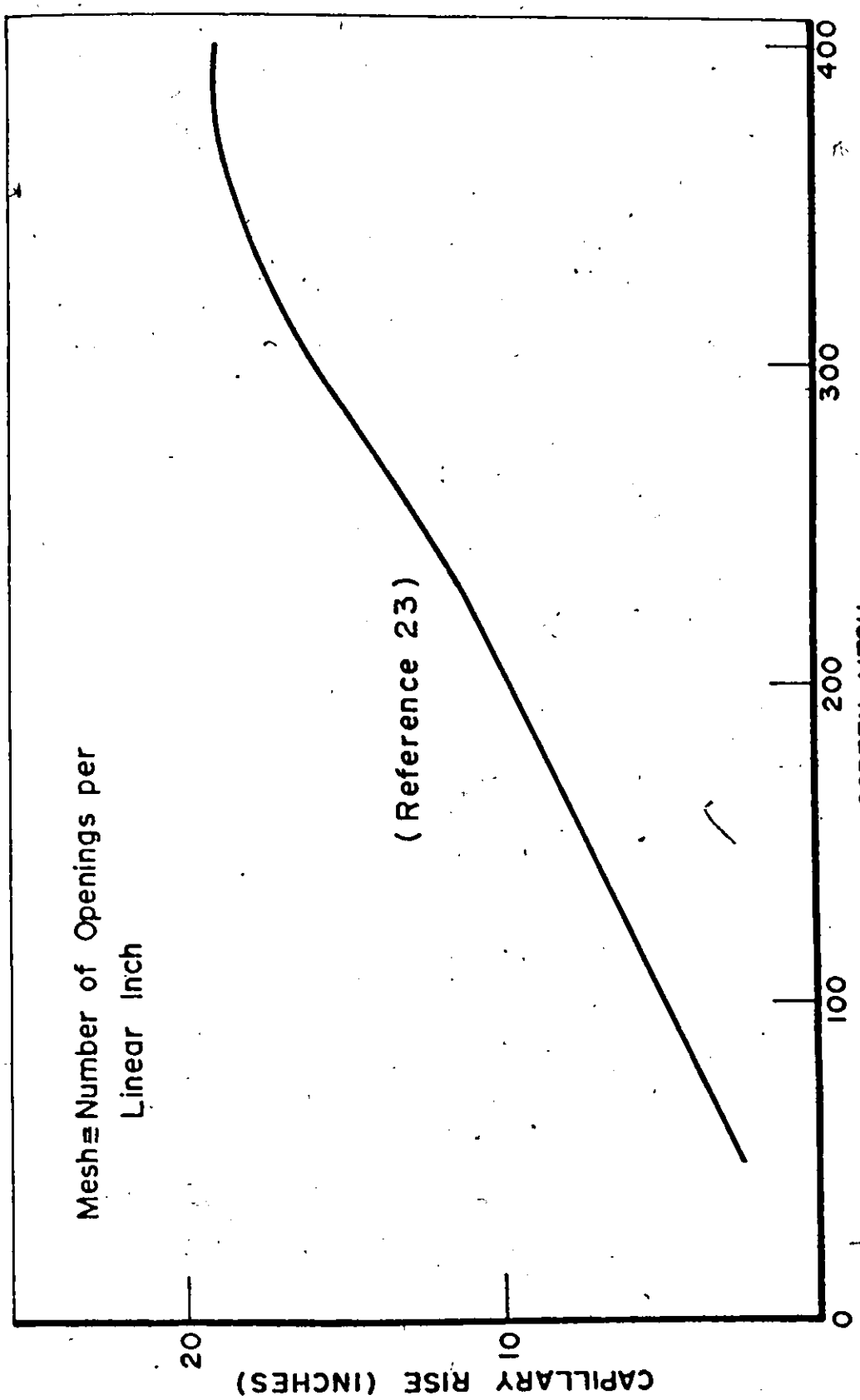

Fig.5 Capillary Rise versus Screen Mesh

In order to determine the amount of distilled water required to saturate the wick, the screen was wrapped around the mandrel, held in shape with tape and the mandrel withdrawn. A simple experiment was then performed by immersing the screen in a measured amount of distilled water and leaving it for a period of time. When the screen was removed, 18.0 c.c. of water was retained by it. This procedure was repeated three times and the same result was obtained. It was decided to load the heat pipe with 24.0 c.c. of water allowing for a 6.0 c.c. extra to ensure proper saturation of the wick. The screen was then unwrapped and dried.

Finally the wood mandrel was installed on the lathe and the screen wrapped around it by turning on the lathe at a low speed and stretching the screen. After removing the mandrel, the screen was spot welded at different axial locations to prevent unwrapping and facilitate installing it in the pipe. The number of layers were counted (16 layers) and the thickness of the wick measured (0.055 inch).

3.5. Preparation and Assembling of the Heat Pipe System

Previous experiments (11, 19, 21, 23) indicated that one of the most important procedures for consideration was the assembly of the heat pipe. The heat pipe should be sealed so that pressure may be built up inside the heat pipe.

Precaution should be taken to prevent contamination of the inside of the heat pipe. Compatibility of materials and cleanliness should also be considered. Contamination and compatibility are important, because if foreign gases collect in the vapor space, the part of the heat pipe occupied by these gases will cease to operate as a heat pipe.

In order to leak test, evacuate and load the heat pipe, a vacuum fill system was installed on the condenser side of the pipe. This system also served in measuring the pressure inside the heat pipe. The system was composed of a T section swagelock connector, connected at one end by a copper tube to a male connector swagelock welded in the condenser end cap. The other two ends of the T section were connected each to a stop valve. One valve led to the pressure gauge, and the other either to the argon bottle for leak and pressure testing, or to the vacuum pump, or finally to a syringe for loading the pipe with the working fluid.

After this system was installed, the heat pipe was leak tested using argon, being an inert gas, to prevent any corrosion in the heat pipe. A great effort was made to completely seal the heat pipe so that no leakage appeared at an argon pressure of approximately 170 p.s.i.g. The pipe was then evacuated until the pressure was 1 mm vacuum, and leak tested under vacuum conditions, by noticing the variation of vacuum with time as given by a mercury column

manometer.

The heat pipe was then loaded with the required amount of water using a syringe. The purpose of the syringe was to avoid any air contamination. Air in the copper tubing was first displaced by the water from the syringe. The syringe flange was then pressed in a teflon tube connected to the copper tubing. High vacuum grease was used to prevent air leakage. Finally the valve was opened to load the pipe. This filling procedure was done while the heat pipe was in a vertical position. After loading the heat pipe with water, the measured vapor pressure was equivalent to the theoretical pressure corresponding to the vapor core temperature in the condenser; thus verifying in part the success of the filling procedure.

Steps taken to assemble the heat pipe and the auxiliary apparatus including the heater and condenser sections are given in Appendix C. Figure 6 and 7 also show intermediate steps in the assembly procedure.

3.6. Operation of the Heat Pipe

After the heat pipe was assembled and filled with the proper amount of water, early tests showed that there was some difficulty in getting the wick to fill properly. This was noticed by the rapid increase in the surface temperature at the evaporator section for a given heat input to the heaters. The system was stopped and the heat pipe was shaken and turned in all directions. This operation

CAPTIONS FOR FIGURES 6 AND 7

A	Cartridge Heater Terminals
B	Evaporator Vapor-Core Ceramocouple
C	Heater Block (4 parts)
D	The Streamlined Heat Pipe
E	Thermocouple Wires
F	Condenser Section
G	Vacuum-Fill System

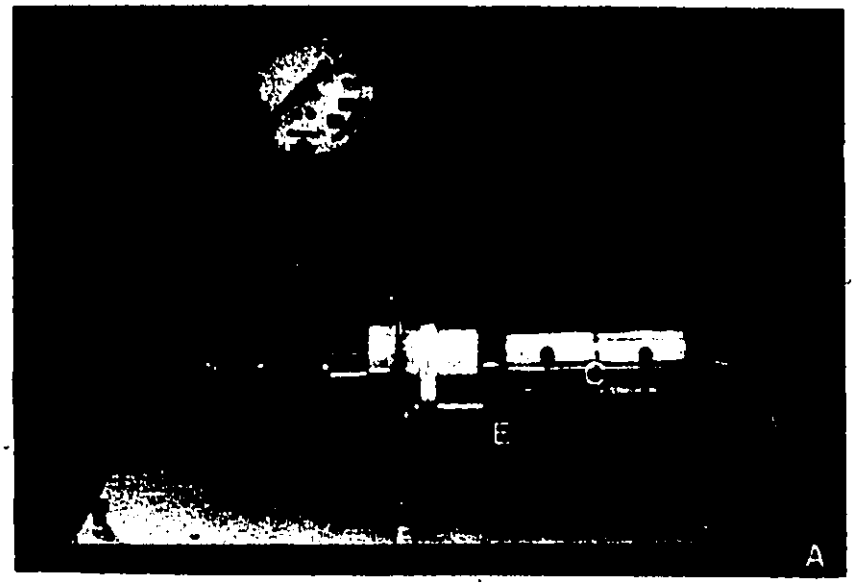

Fig. 6 The Apparatus Showing Mainly the Heater Block, the Condenser and the Vacuum-fill System.

Fig. 7 The Thermocouples Welded on the Top Surface of the Heat Pipe before Installing the Heater Block.

was done periodically before each test to ensure that the wick was more or less uniformly saturated by the water.

To obtain a common starting point for each series of tests, the pressure inside the pipe was checked. The pressure in the pipe at room temperature should be equal to the pressure of saturated water vapor at that given temperature. This was verified before each test and no deviation was noticed, indicating that the heat pipe was completely sealed and no possibility of contamination from external sources to the heat pipe when left overnight or longer.

The first steps of the operation of the heat pipe consisted of warming up the potentiometer and the recorder to ensure good stability. The potentiometer and recorder were then calibrated. Readings were made on all thermocouples to ensure proper operation. The condenser water flow was started, and when steadiness was achieved the pipe heaters were energized and the pipe commenced operation.

At each power level, the transient temperature variation was observed on the recorder until steady state condition was achieved. This was noted by a stabilization of the surface temperature measurements, and the inlet and outlet water temperatures to the calorimeter. For a power increment of 25 watts the time required to reach steady state condition was about 90 minutes. The staring time was somewhat longer (2 to 3 hours). Figure 8 shows the variation

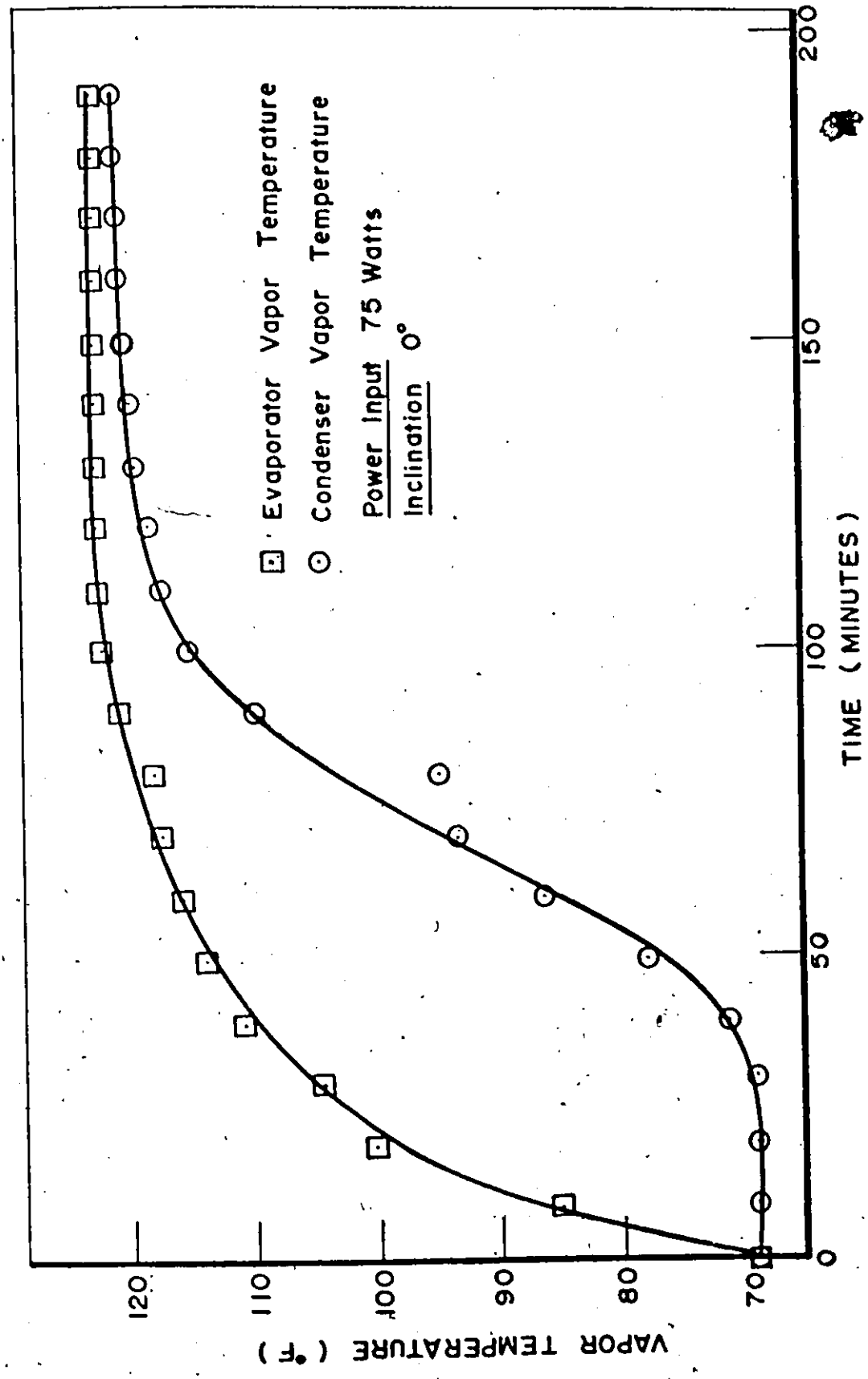

Fig.8 Vapor Temperature–Transient Variation

of the vapor core temperature in the condenser and in the evaporator with time, for the heat pipe installed in the horizontal direction during starting at a power of 75 watts.

The coincidence of the two vapor temperatures is an important criterion for a successful heat pipe operation. This was verified during all tests meaning that the heat pipe was working nearly isothermally in the vapor core, and so resulting in a higher equivalent thermal conductivity. Actually there was a large axial surface temperature drop between both ends, due to the radial conduction temperature gradient in the pipe wall and the liquid-wick matrix at the evaporator and condenser respectively.

The upper limit of heat flux was determined by dryout in the evaporator wick. Dryout was a result of insufficient condensate being delivered by the wick to the evaporator end. The onset of this condition was detected by the rapid increase of the surface temperature at the far end of the evaporator. This was generally the first indication of approaching complete dryout of the evaporator wick, with the dryout line advancing from the evaporator to the condenser. Once this condition was reached, the power to the heaters were turned off, and the water flow was left for a period of time to assist in cooling the heat pipe.

CHAPTER IV

EXPERIMENTAL RESULTS AND ANALYSIS

4.1. Performance Data Summary

The streamlined heat pipe performance data summary at the four different orientations are tabulated (Tables IV through VII) in Appendix D. For the sake of analysis and later discussions, Table IV, presenting the performance data of the heat pipe in the horizontal direction, is repeated in this section.

The first four rows to Table IV, present at each heat input level "Q_i", the measured water flow rate through the calorimeter in cubic centimeters per minute, and the water inlet and outlet temperature in ^{o}C. The heat output Q_o in watts and the efficiency of heat transmission were calculated and are shown in rows 5 and 6. The vapor core temperature in the condenser section T_{vc} is given in row 7; the measured condenser vapor pressure P_{vc} is tabulated in row 8, while the saturation pressure corresponding to the measured vapor core temperature in the condenser is shown in row 9. Rows 10, 11 and 14 give the temperature drops in ^{o}F in the vapor core ΔT_v, across the adiabatic section ΔT_a and along the heat pipe ΔT_p respectively; this corresponds to (T1-T2), (T12-T15) and (T3-T18) in Figure 2. Rows 12 and 13 show the axial heat transferred by conduction through the pipe wall as an absolute value in watts Q' and as a percentage

Power Input (Watts)	75	100	125	150
Water Flow Rate (c.c./min.)	280	325	325	325
Water Inlet Temperature (^{o}C)	20.0	18.7	17.5	16.3
Water Outlet Temperature (^{o}C)	23.5	22.8	22.5	22.5
Power Output (Watts)	69.38	94.34	115.05	142.66
Efficiency (%)	92.51	94.34	92.04	95.1
Condenser Vapor Temperature (^{o}F)	121.0	126.0	131.0	134.0
Condenser Vapor Pressure (in Hg)	3.5	4.0	4.5	5.0
Pressure (Steam Table) (inch)	3.3	4.06	4.64	5.03
Vapor Temperature Drop (^{o}F)	2.0	0.5	0.0	0.0
Adiabatic Section Temperature Drop (^{o}F)	45.75	54.5	61.15	68.7
Axial Heat Conduction (Watts)	2.16	2.56	2.88	3.23
Axial Heat Conduction Percentage (%)	3.11	2.71	2.50	2.26
Heat Pipe Temperature Drop (^{o}F)	70.6	82.45	96.3	107.6
Equivalent Thermal Conductivity (BTU/hr.ft.^{o}F)	659.4	767.8	801.6	890.6
Power Output per lbs. for Heat Pipe (Watts/lbs.)	138.8	188.7	230.1	285.3
Equivalent Power Output per lbs for Copper Rod (Watts/lb.)	12.97	15.15	17.69	19.74

Table IV Performance Data of the Heat Pipe at $\alpha = 0^{o}$

Table IV Continued

Power Input (Watts)	175	200	225	250
Water Flow Rate (c.c./min.)	325	360	360	340
Water Inlet Temperature (^{o}C)	15.5	14.8	15.0	15.0
Water Outlet Temperature (^{o}C)	22.6	22.1	23.2	24.5
Power Output (Watts)	163.37	186.06	209	235.41
Efficiency (%)	93.35	93.03	92.89	94.16
Condenser Vapor Temperature (^{o}F)	139.0	146.0	156.0	165.5
Condenser Vapor Pressure (in Hg	5.5	6.5	8.0	10.0
Pressure (Steam Table) (inch)	5.73	6.85	8.76	10.9
Vapor Temperature Drop (^{o}F)	0.0	0.0	0.0	0.0
Adiabatic Section Temperature Drop (^{o}F)	77.25	91.6	113.2	119.05
Axial Heat Conduction (Watts)	3.64	4.32	5.54	5.61
Axial Heat Conduction Percentage (%)	2.22	2.32	2.55	2.38
Heat Pipe Temperature Drop (^{o}F)	123.9	144.2	162.7	179.6
Equivalent Thermal Conductivity (BTU/hr.ft.^{o}F)	884.7	865.8	861.9	879.5
Power Output per lbs. for Heat Pipe (Watts/lbs.)	326.7	372.1	418.0	470.8
Equivalent Power Output per lbs for Copper Rod (Watts/lb.)	22.77	26.50	29.90	33.01

of the total heat output Q'%. Tabulated in the last three rows respectively are the equivalent thermal conductivity of the heat pipe k_{eq} in BTU/hr.ft.^{o}F, the heat output per unit weight of the heat pipe and finally the equivalent heat output per unit weight of a solid copper rod of comparable size.

4.2. Axial Temperature Distributions

To achieve higher thermal conductivity, the temperatures prevailing in the vapor core of the heat pipe should be constant in the axial direction, except for a very small temperature gradient necessary to drive the vapor from the evaporator to the condenser. If heat is added and rejected at a constant rate, it is expected that both the evaporator and the condenser surfaces will have isothermal temperature profiles, neglecting any axial conduction temperature gradients. These two constant temperatures in the evaporator and condenser are dictated by the heat resistance path existing between the heat pipe outside surface and the wick inside surface (liquid-vapor interface).

For each test, before any heat was applied, the axial temperature profile was measured. It was found in all runs that the error was less than 1% for all thermocouples except for thermocouple number 5 (Figure 2). For example, in the horizontal direction test, the minimum and maximum temperatures measured at room temperature were 70.9^{o}F and 71.4^{o}F respectively, the temperatures at point 5 was 69.9^{o}F.

Figures 9 through 12 show the axial temperature distributions obtained for all tests as a function of orientation and heat input. Also shown on the left hand side of the figures are the vapor core temperatures measured in the evaporator.

In order to compare the experimental and the theoretical temperature distributions, Appendix E presents an analysis of the temperature gradients in a cylindrical heat pipe. A sample calculation is also given for the streamlined heat pipe installed in the horizontal direction at a heat input of 150 watts. In these calculations the streamlined heat pipe was treated as a circular one having the same cross-section area. The theoretical temperature distribution was based on the same vapor core temperature found by experiment. Figure 13 shows the theoretical and the experimental axial temperature profiles for this case.

Examining Figures 9 through 13, the temperature profile in the condenser for all tests was nearly isothermal, thus confirming the theory. In some tests however, the temperature at point 15 was less than expected, due to the fact that the cooling water entered the calorimeter near this point. In the evaporator, a relatively high temperature gradient ensued and some of the temperature readings deviated from the mean profile (or the theoretical model). This fact was more pronounced in the horizontal direction and at high power levels, for all inclinations.

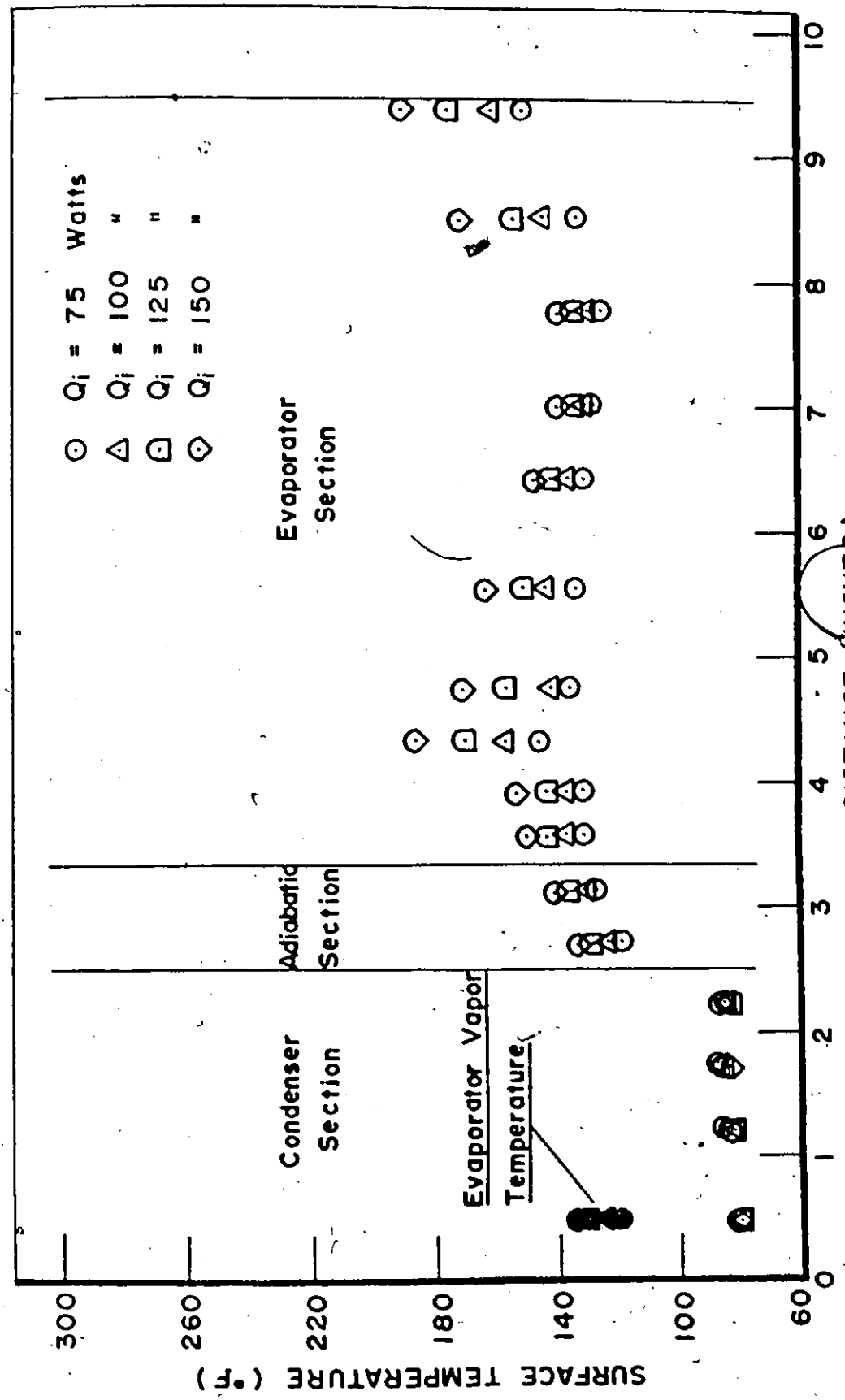

Fig. 9a Axial Temperature Distributions at various Heat Inputs for $\alpha = 0°$

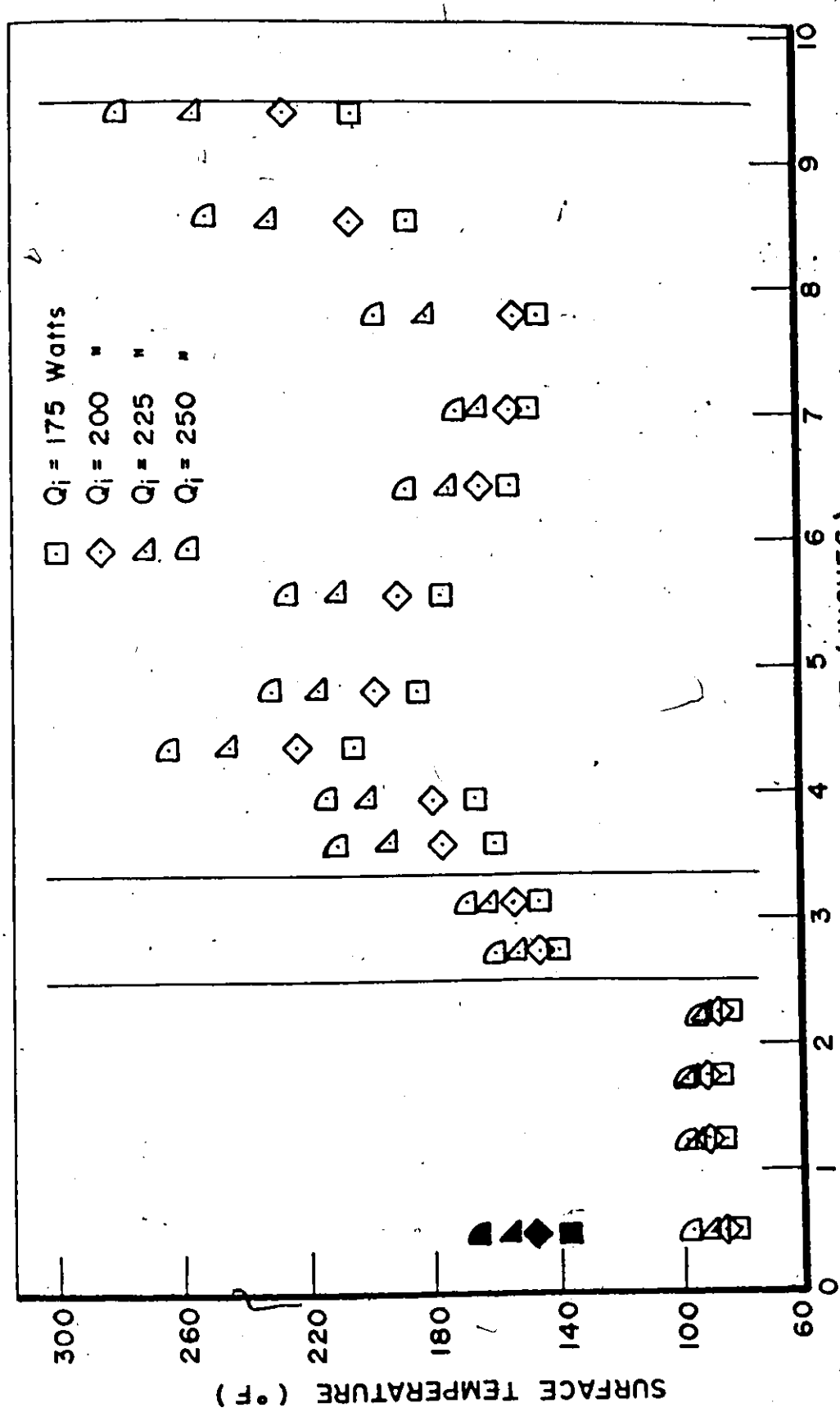

Fig. 9b Axial Temperature Distributions at various Heat Inputs for $\alpha = 0^{\circ}$

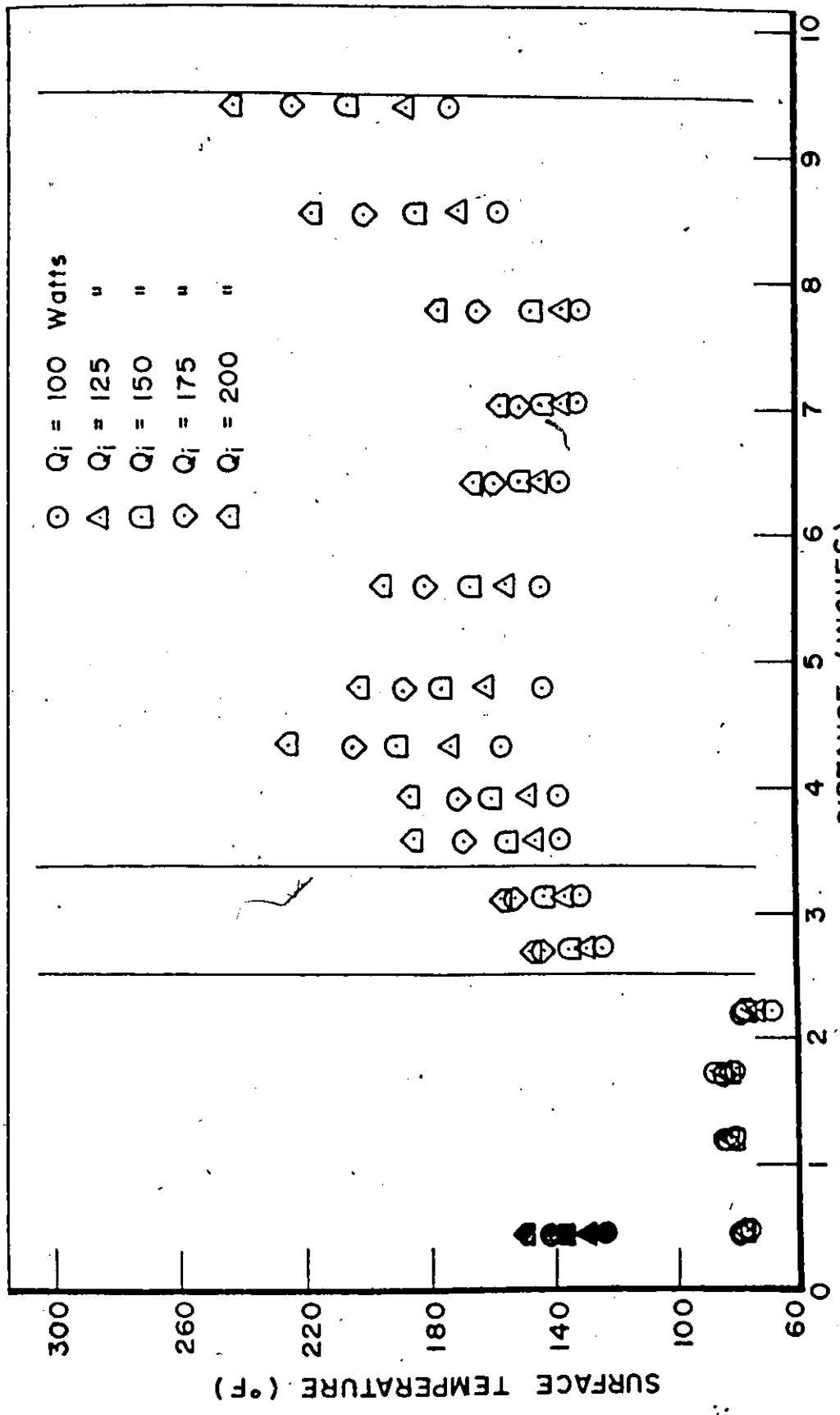

Fig.10 Axial Temperature Distributions at various Heat Inputs for $\alpha=15°$

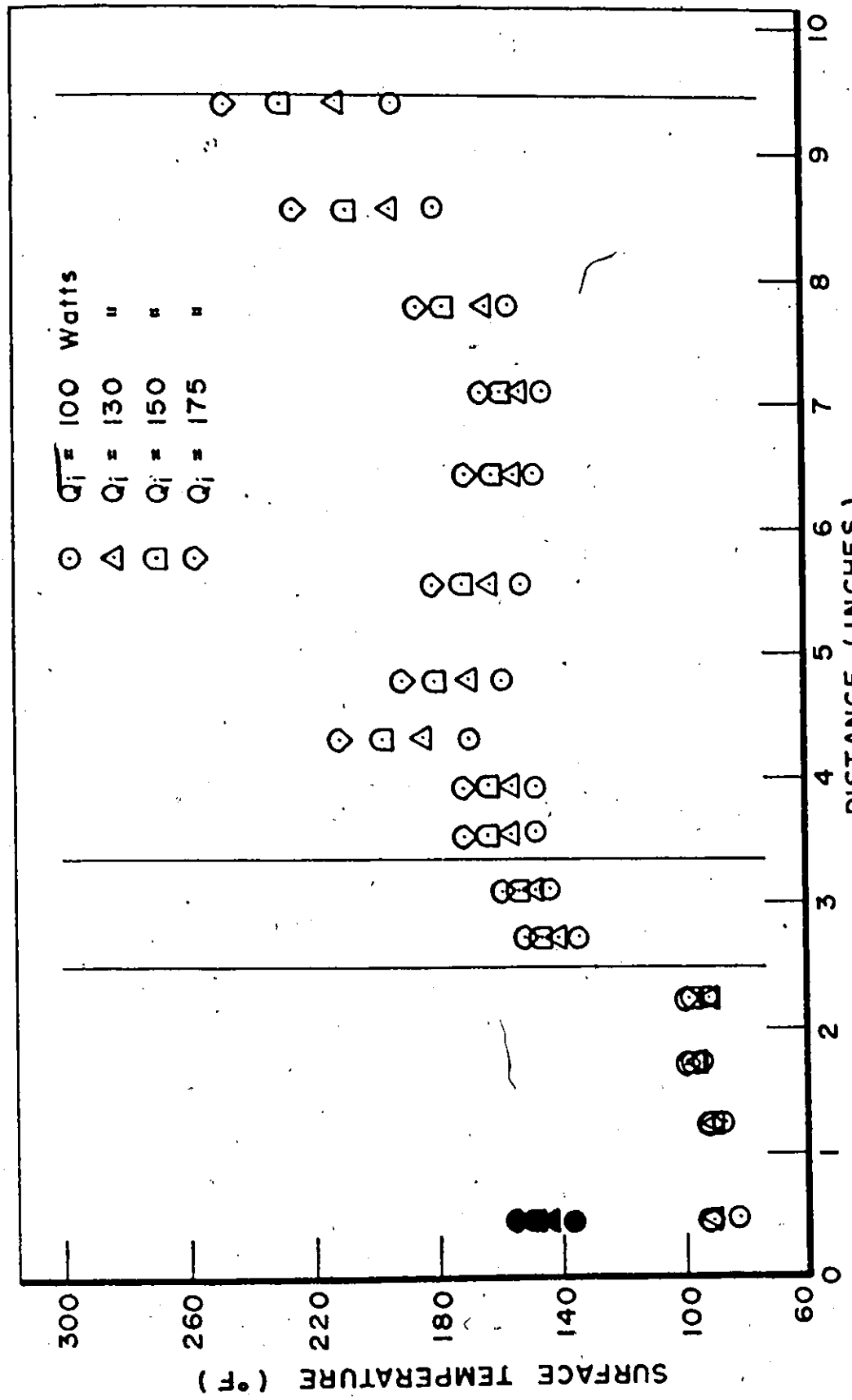

Fig.11 Axial Temperature Distributions at various Heat Inputs for $\alpha=30°$

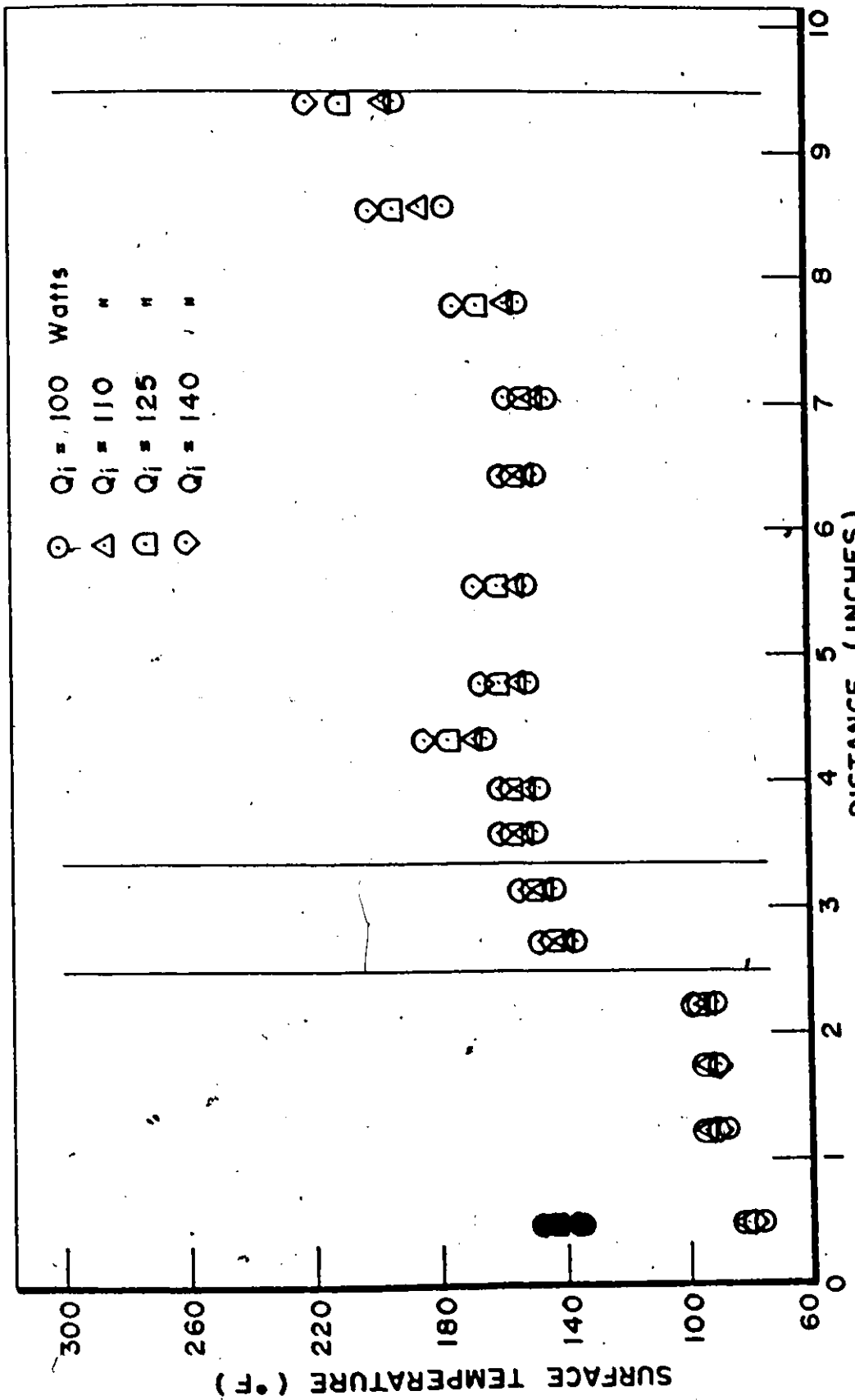

Fig. 12 Axial Temperature Distributions at various Heat Inputs for $\alpha = 45°$

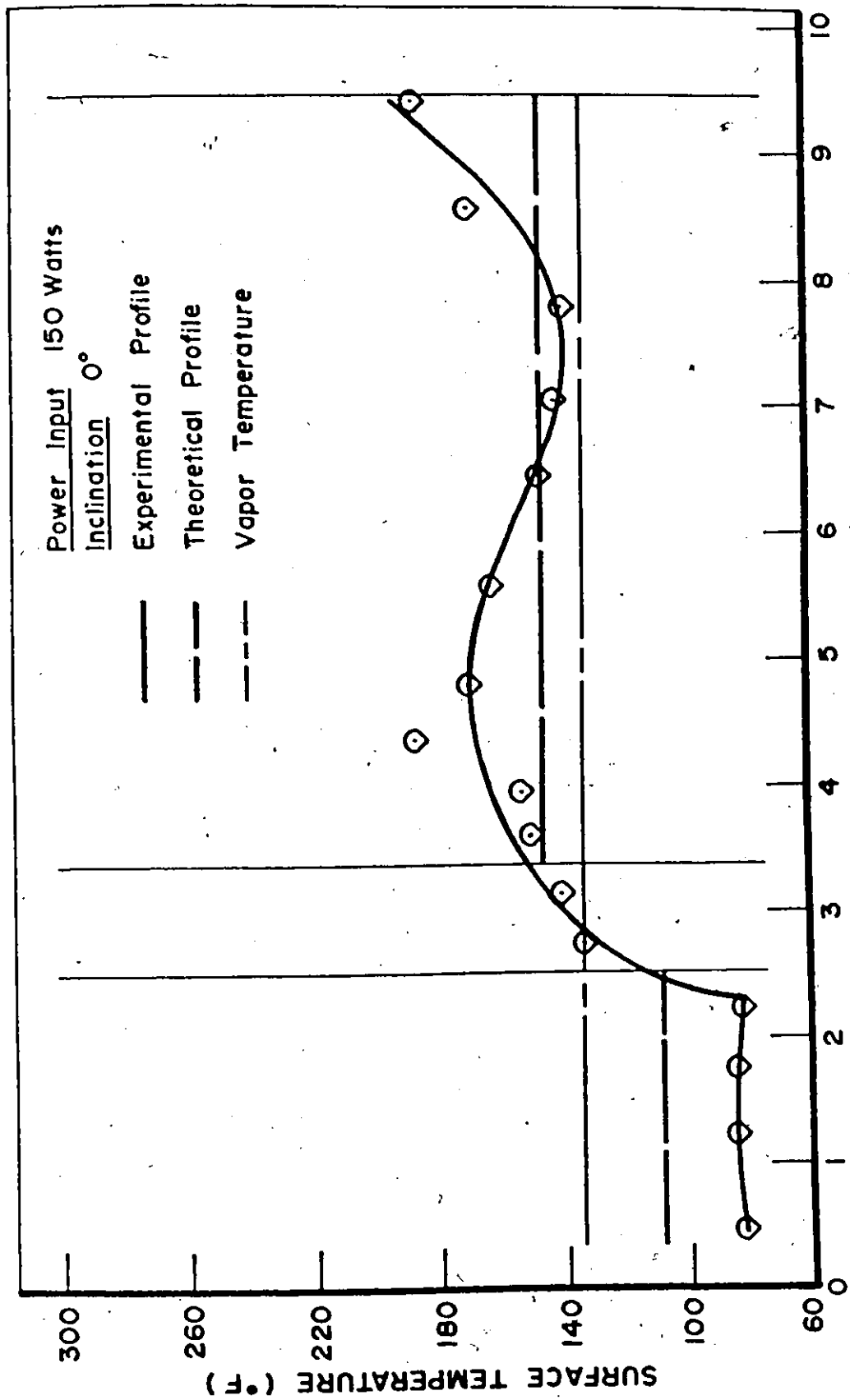

Fig.13 Experimental & Theoretical Axial Temperature Profiles

Feldman and Whitlow (18) had found similar temperature profiles in the evaporator region of an 18 inches long cylindrical heat pipe using water as the working fluid and 100 mesh copper screen as the wick. The evaporator length was 9 inches and the thermocouples were located at approximately one inch intervals. Further comparison with other experiments proved largely inconclusive since in many cases the longitudinal temperature profile was obtained with only a few thermocouples.

The temperature gradients and deviations found could be attributed to several factors. The first factor may be that the screen did not wet well, and the water was not saturating the wick uniformly. The second factor could be due to the contact resistance between the pipe wall and the wick material. The wick was only held against the pipe wall by virtue of its own resilience. A third factor could be due to axial conduction temperature gradient through the pipe wall and saturated wick. Finally the higher temperatures found at points 3, 4 and 10 as compared to other temperatures, could be from the fact that the thermocouples were exposed to some fraction of the inside heater block surface temperatures. Any small air gap between the heater block and the heat pipe would justify this argument.

By comparing the temperature profiles at the different inclinations, it was noticed that higher temperatures existed at higher inclinations. This agreed with the results obtained by Neal (11), who held the power input constant

and lowered the condenser in increments to study the effect of inclination on temperature profiles for a water heat pipe. The main reason for the increase in temperature may be due to the partial saturation of the wick when the evaporator was raised above the condenser.

4.3. Heat Output versus Heat Input

By measuring the water flow rate in c.c./min. and the water inlet and outlet temperature in ^{o}C, the heat output rate could be computed at each power input.

A typical heat output versus heat input relationship at different inclinations is shown in Figure 14. It is clear that the data could be correlated by a straight line whose slope is 0.925. This means that the average efficiency of heat transmission was 92.5%. The differences between the heat inputs and outputs are the heat losses to the atmosphere, mainly at the hot section of the heat pipe. For the heat pipe installed horizontally, at a heat input of 150 watts, the heat output was 142.66 watts. The heat losses due to natural convection from the hot end was estimated to be 5.57 watts. This was based on a measured temperature difference between the insulation outside surface and the atmosphere of 21.5^{o}F. The heat transfer coefficient was taken to be 0.69 BTU/hr.ft.^{o}F (35).

4.4. Effect of Inclination on Maximum Heat Transfer

At moderate power levels, the main limiting factor of the operation of a heat pipe is the capillary or wicking

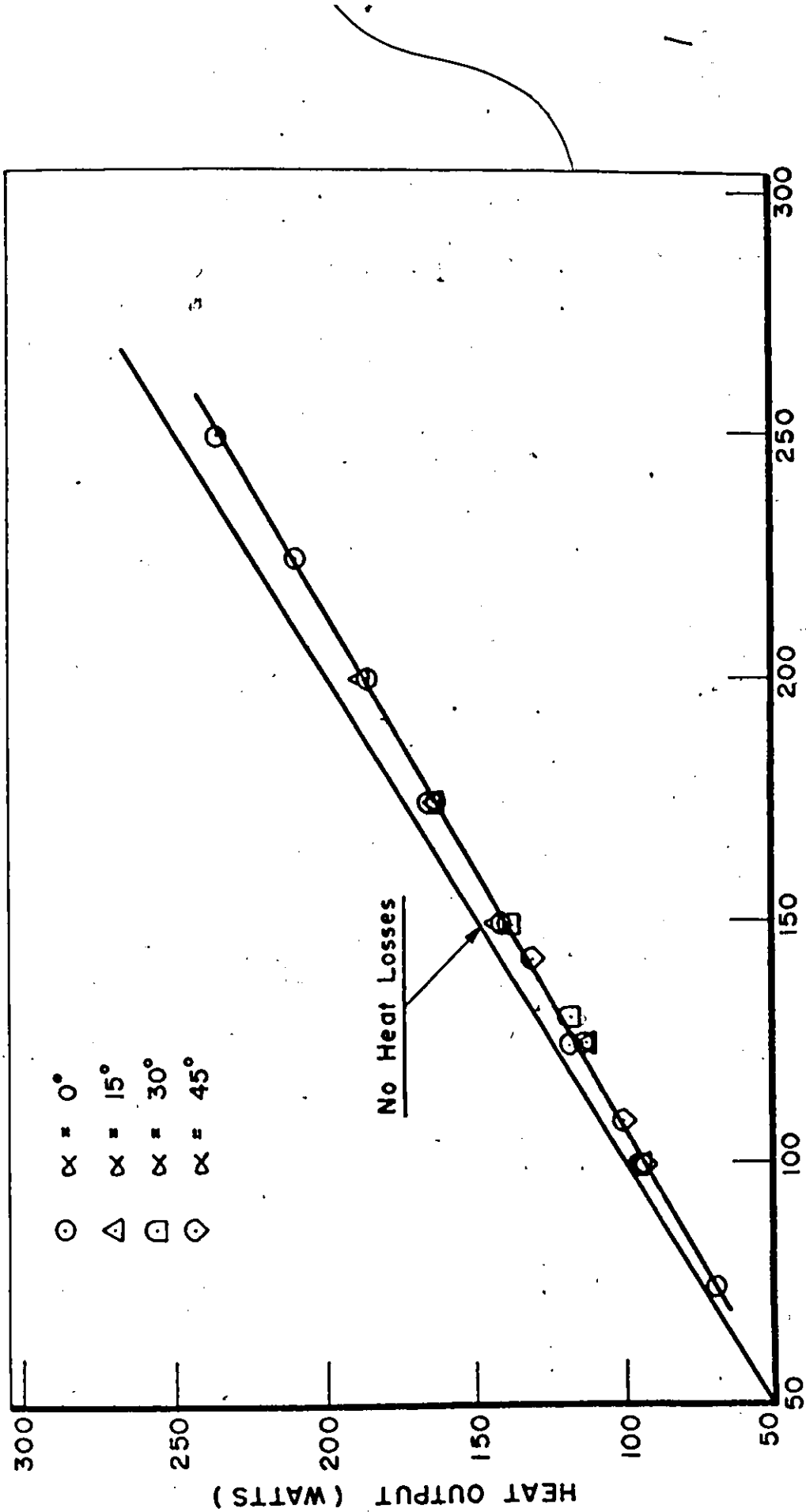

Fig.14 Heat Output versus Heat Input

limit. This condition is reached when a given heat flux causes the liquid in the liquid wick matrix to evaporate faster than it can be supplied by capillary pumping in the wick. Once this condition occurs, the liquid-vapor meniscus continues to recede into the wick until all of the liquid has been depleted. A dryout condition is reached in the evaporator wick, and which is detected by the rapid increase in the container temperature. This normally ends the operation of the configuration as a heat pipe.

Figure 15 presents the variation of the maximum heat transferred by the streamlined heat pipe as a function of inclination (α). Also shown are the theoretical results obtained using Equation (B.1).

The experimental data are presented by two curves, the heat input and the heat output curves respectively. For the heat input curve, the term "stable" refers to conditions where thermal equilibrium was attained, while "unstable" refers to conditions where no stabilization of the temperatures were reached. In the horizontal direction the maximum heat input was 250 watts, while in the vertical direction at a heat input of 25 watts no thermal equilibrium was attained. This dropping characteristic agreed with previous investigations (11, 21, 32). As the evaporator was raised above the condenser level, the required pumping pressure increases due to the gravity forces. Thus the maximum capillary pressure, which could be provided by the screen mesh was reached at lower power levels.

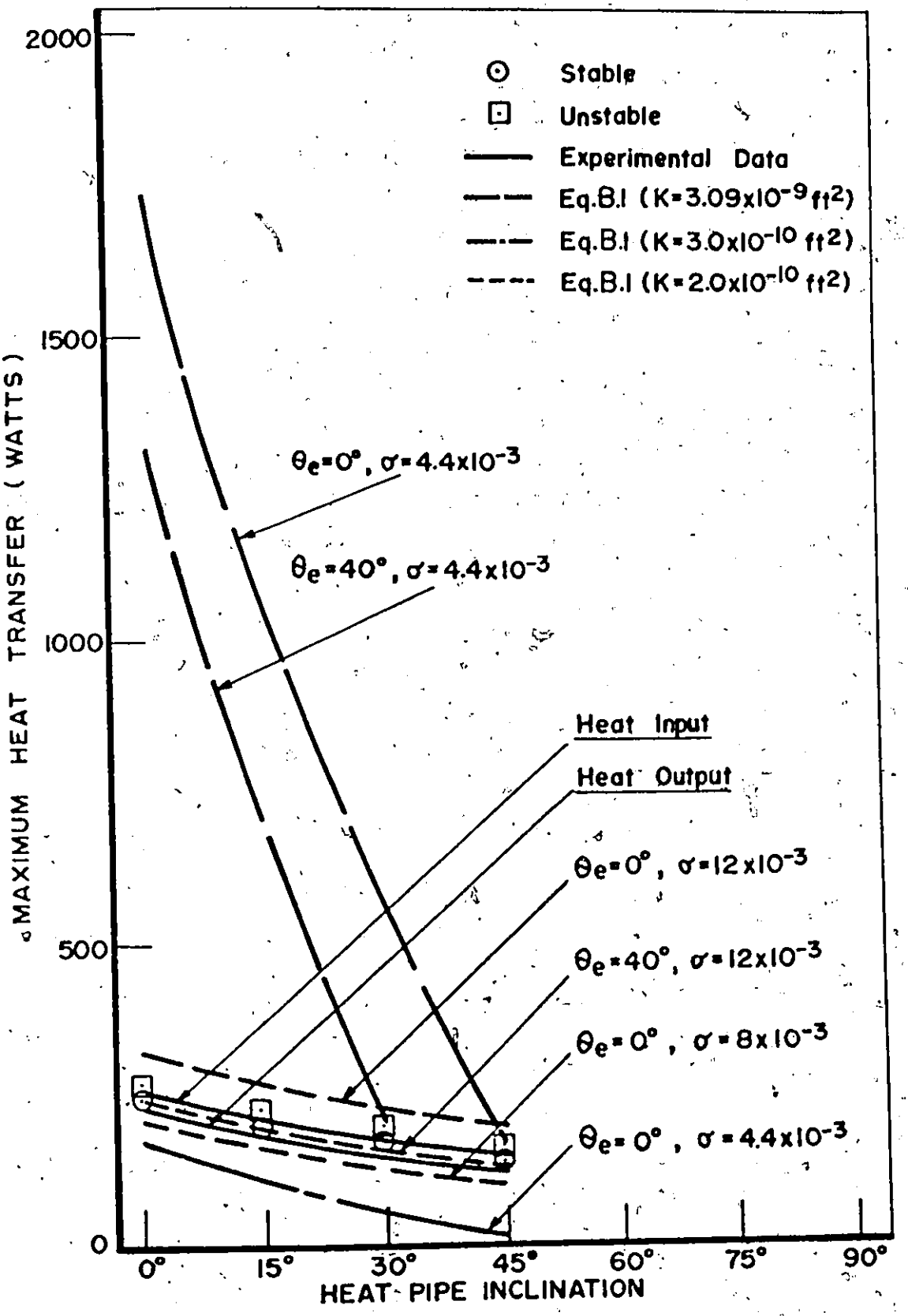

Fig.15 Effect of Inclination on Maximum Heat Transfer

The computer program used in Appendix B for calculating the maximum heat transfer by cylindrical heat pipe as a function of operating temperatures and wick thicknesses, was modified to compare the experimental and theoretical results. The main aim of this theoretical study was to find out the effect of selected parameters on heat pipe performance, and to estimate their values which may represent the experimental results. The streamlined heat pipe was treated as a circular one having the same cross-section area with a wick thickness given by r_3/r_2 equal to 0.865 (Appendix E). The maximum heat transfers were calculated by varying four parameters: the inclination (α), the evaporator contact angle (θ_e), the wick permeability (K), and the surface tension (σ). The operating temperatures used in the computations were those measured experimentally at dryout conditions for the corresponding orientations.

From the results obtained, it is seen that if a heat pipe is to be designed to transfer high power at a particular inclination (for example $\alpha = 0^o$ or 15^o) a wick of high permeability should be used. However, if a heat pipe is required to transfer moderate power at all inclinations, a wick of relatively lower permeability may be chosen. The experimental results as given by the heat input and output curves in Figure 15, may be represented by Equation (B.1) if the permeability is 2.0×10^{-10} ft^2 and the product ($\sigma \times \cos \theta_e$) is approximately 9×10^{-3} lb_f/ft. This may correspond to values of θ_e ranging from 0^o to 40^o, and σ from 8×10^{-3} to 10^{-2} lb_f/ft.

4.5. Vapor Core Pressure-Temperature Relation

Figure 16 shows the variation of the theoretical and measured vapor pressure in the condenser, with the vapor core temperature (or saturation temperature) in the consensor.

With the pressure gauge used, it is seen that the measured vapor pressures agreed reasonably well with the theoretical pressures as obtained from the steam tables (33). This agreement indicated the success of the sealing procedure: no measurable leakage occurred when the heat pipe was left overnight or longer. If air entered the apparatus the heat transfer effect due to the vapor would be reduced in the same fashion as seen in a steam condenser with air contamination.

4.6. Vapor Temperature Variation with Heat Input

The vapor temperature, or the operating temperature as it is sometimes called, of the heat pipe is essentially determined by the coupling of the heat pipe to the heat source and the heat sink. The vapor temperature adjusts itself in such a way so that the temperature drop across the liquid-wick matrix and the container wall in the evaporator and condenser is adequate to transfer the given heat flow from the heat source to the heat sink. In other words, the absolute vapor temperature is established in response to the temperatures imposed on both the evaporator and condenser by the source and sink. The temperatures at the outside wall of the heat pipe may be either fixed or floating depending

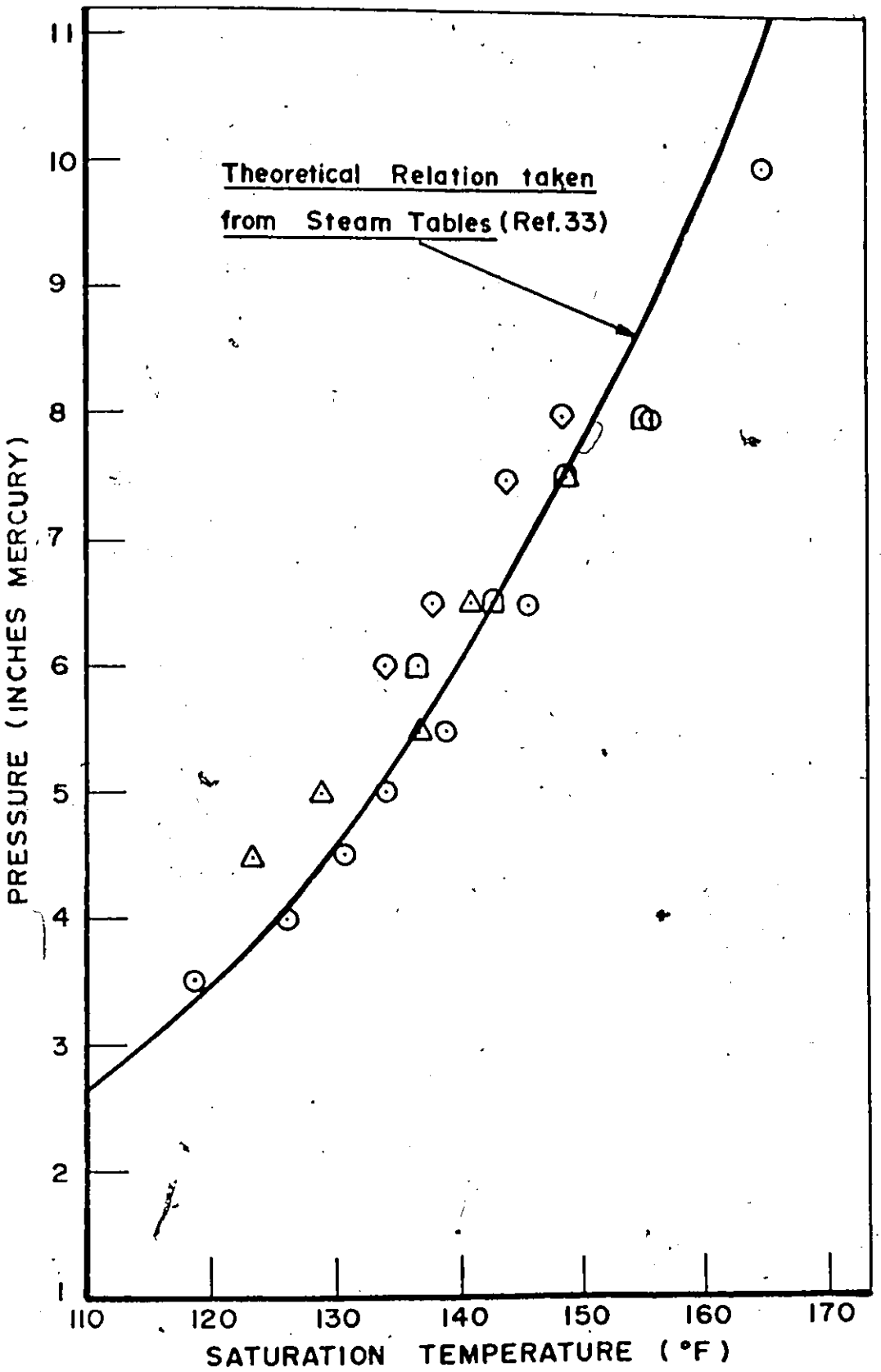

Fig. 16 Vapor Core Pressure–Temperature Relation

on the type of constraints imposed by source or sink.

In the experiments conducted on the present heat pipe, the heat sink was kept at a fixed temperature governed by the temperature of the cooling water, and the source temperature was allowed to float with the applied heat flux. Consequently the vapor temperature floated, taking an average value between the source and the sink temperature. Figure 17 shows the variation of the evaporator vapor temperature with heat input for the different inclinations.

Up to a heat input of 175 watts, the data could be presented by straight lines, but at higher powers (for $\alpha = 0^{\circ}$ and 15°) the rate of increase of vapor temperature with input power tended to become higher. Also, the curves indicated that for a certain heat input, the vapor temperature increased with inclination. The two previous conclusions could be drawn from the shape of the axial temperature distribution curves, which in turn affected the rate of change of vapor temperature with heat input.

The effect of heat sink temperature (cooling water temperature) on the heat pipe operating temperature was clear when one observed the large increase of data for $\alpha = 30^{\circ}$ and 45° over those for $\alpha = 0^{\circ}$ and 15°. This was due to the fact that the average water inlet temperature for $\alpha = 0^{\circ}$ and 15° was $16^{\circ}C$, compared to $20^{\circ}C$ for $\alpha = 30^{\circ}$ and 45°. Normally one would have expected for a constant input water temperature, the evaporator vapor temperature stability limits, to occur in a consistent fashion with an increase in inclination.

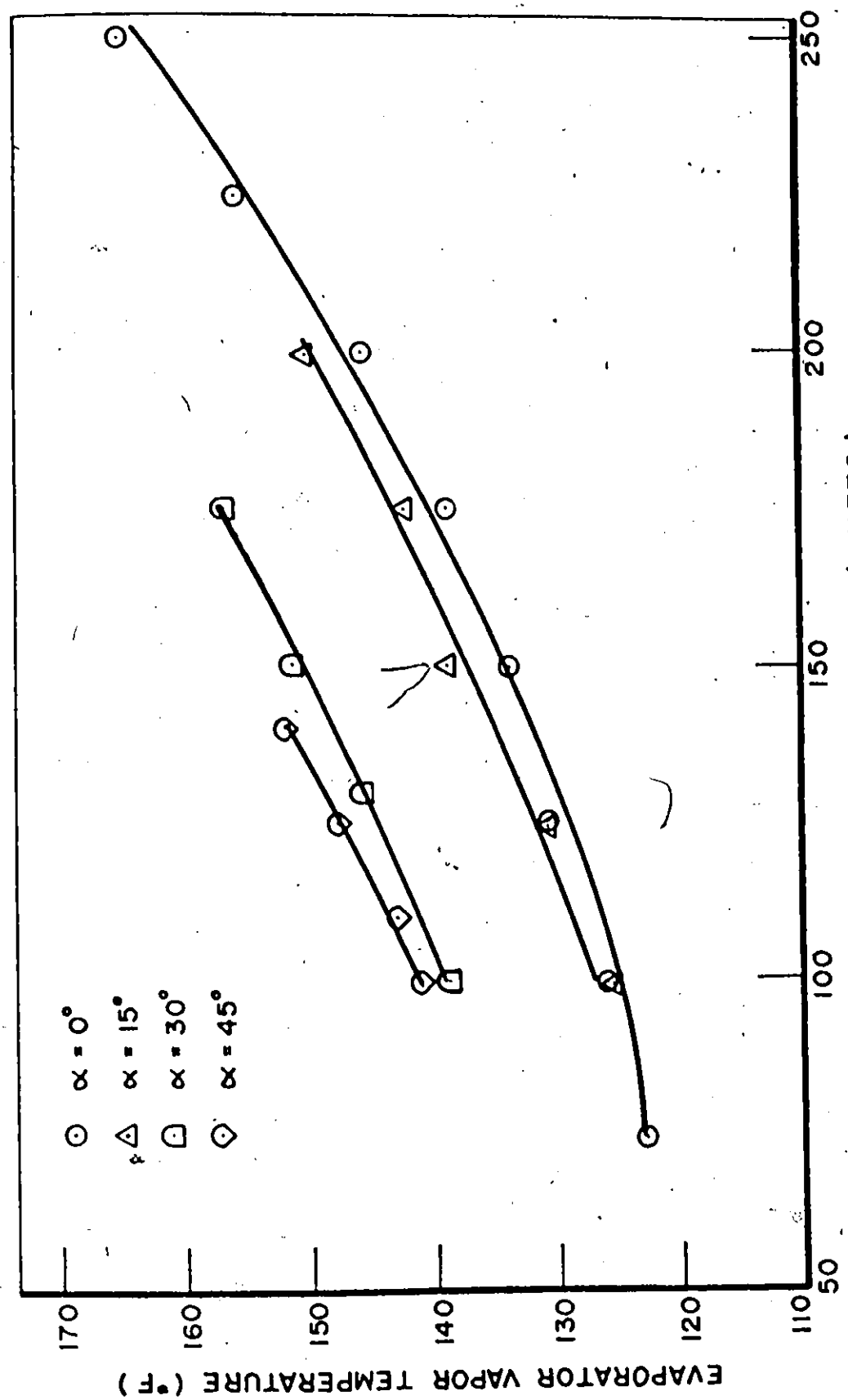

Fig.17 Vapor Temperature Variation with Heat Input

Another reason for the differences between the curves shown in Figure 17, could be attributed to the increase of vapor temperature drop between evaporator and condenser with inclination (Appendix D, row 10 in Tables IV through VII).

The previous analysis is applicable for any curve showing the variation of a certain parameter with the vapor core temperature.

4.7. Axial Heat Conduction

The axial heat conduction through the pipe wall has been neglected in many of the existing analysis. Considering the overall thermal performance, however, axial wall conduction might become an important mode of energy transfer as it interacts in a direct manner with various other modes of heat transfer in a heat pipe.

The heat transferred by axial conduction was computed for all the data obtained. In these calculations the axial conduction was considered only through the pipe wall of the adiabatic section, thus neglecting any axial heat conduction through the liquid-wick matrix and the evaporator section respectively.

Applying Fourier's conduction equation over the adiabatic section of the heat pipe one may write

$$Q = - k A (\Delta T/\Delta X)$$

where: k is the thermal conductivity of the pipe material
= 24.67 BTU/hr. ft.^{o}F for the temperature range

from $32^{\circ}F$ to $212^{\circ}F$ (34).

A is the cross section area of the pipe wall = 0.098 in^2

ΔT is the temperature drop across the adiabatic section = T12-T15.

ΔX is the distance between thermocouples 12 and 15.

hence $Q' = 4.72 \times 10^{-2} \Delta T_n$ watts.

We see from this equation, that if the pipe was not loaded with a working fluid, a temperature difference of $2090^{\circ}F$ would be required to transfer a heat load of 100 watts.

The values of the axial heat conduction and percentages from the total heat transferred have been tabulated in Appendix D. The average percentage of axial conduction was approximately 2.5% of the power output, showing that the contribution of axial conduction to the total heat transferred was quite low.

4.8. Temperature Drop between the Evaporator and the Condenser Sections

Theoretically the heat pipe has a nearly isothermal axial temperature profile in the vapor (1, 2, 11, 31). However, in the condenser, there is a temperature rise from the heat sink to the liquid-vapor interface which is of a magnitude that will transfer the latent heat given up through the working fluid-wick matrix and the pipe wall to the sink. In the vapor space, there is a temperature rise from the condenser to the evaporator which is of a magnitude that produces a vapor pressure difference large enough to overcome

the resistance to vapor flow. In the evaporator, there is a temperature rise from the vapor space to the energy source which is large enough to overcome the resistance to heat flow. These transport processes determine the total temperature drop, from source to sink, over the heat pipe.

In Figure 18, the temperature drop along the heat pipe between the extreme ends was plotted versus the heat input. The temperature drop varied linearly with heat input, and as expected from the previous curves (Figures 9 to 13) the temperature gradient becomes more pronounced as the evaporator was raised over the condenser. Also the same factors discussed in section 4.2 apply here, thus explaining the relatively large temperature drops obtained.

If we compare the theoretical and the experimental temperature drop, taking as an example the heat pipe installed in the horizontal direction at an input power of 150 watts, the theoretical drop was 37.97°F (Appendix E) compared to an experimental drop of 107.4°F between the extreme ends, and 70°F if we considered average temperatures in the evaporator and condenser respectively.

4.9. Performance of the Streamlined Heat Pipe Compared to that of a Solid Conductor

Because the heat pipe has a fraction of the weight and several hundred times the heat transfer capability of metals, it appears to provide ideal solutions to almost a limitless number of thermal transport problems.

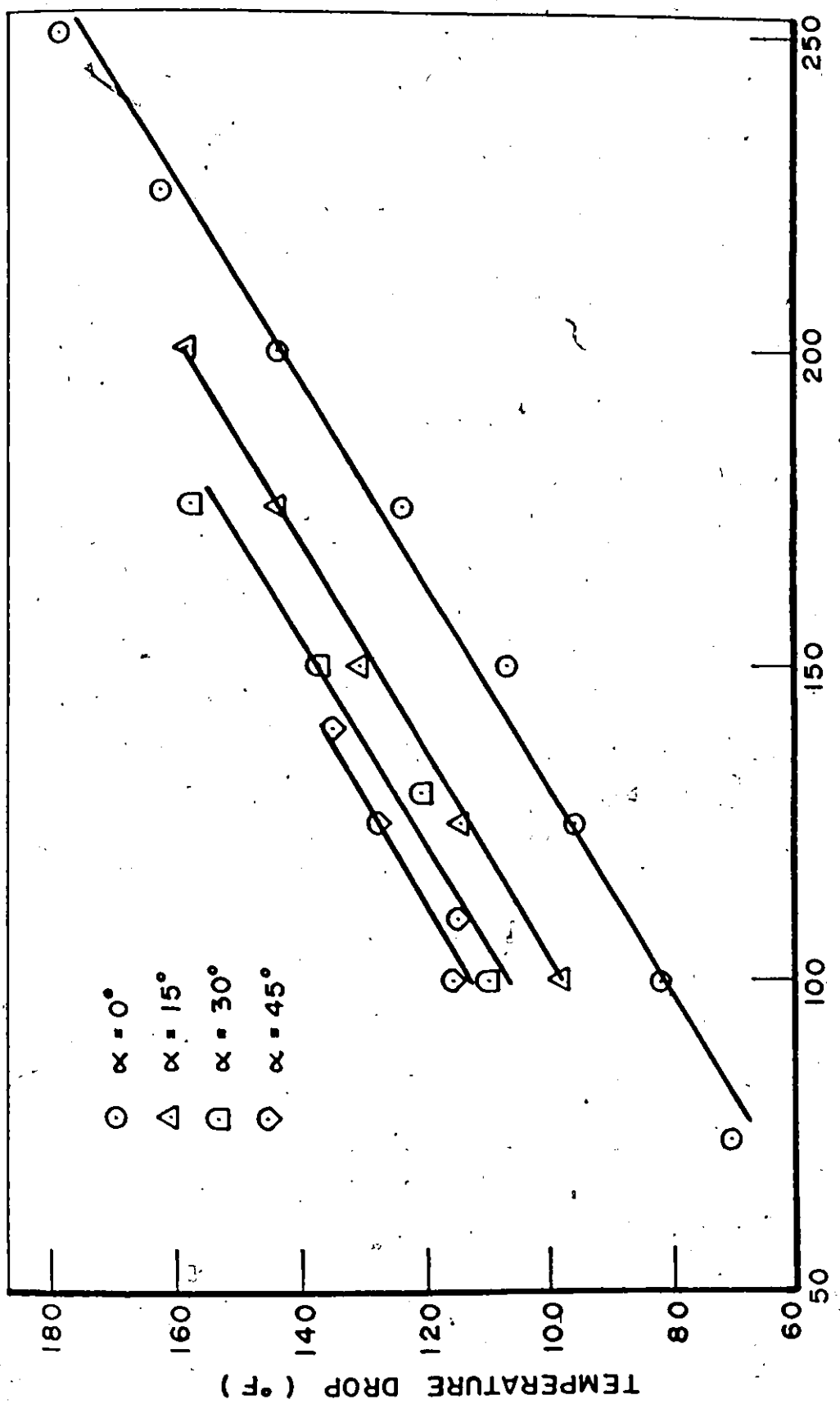

Fig.18 Temperature Drop between the Evaporator & Condenser Sections versus Heat Input

In this section, the performance of the streamlined heat pipe, mainly characterized by its equivalent thermal conductivity and its specific output, is compared to a similar solid conductor taking pure copper as a base of comparison.

a. Equivalent Thermal Conductivity

The equivalent thermal conductivities of the streamlined heat pipe were computed for all the heat inputs at the four different orientations. Row 15 of the performance data (Appendix D), provides these values, and in Figure 19 they have been plotted against the heat pipe operating temperature, together with the thermal conductivity of pure copper.

Applying Fourier's conduction equation in a similar manner to that shown in section 4.7, where:

Q is the axial heat transferred (output power) in watts.

k is the heat pipe equivalent thermal conductivity in BTU/hr.ft^{o}F.

A is the heat pipe cross section area = 0.58 in^2.

ΔT is the temperature drop between the extreme ends of the heat pipe = (T3-T18).

ΔX is the heat pipe length = 9.375 inches.

we obtain $k_{eq} = 671\ (Q_o/\Delta T_p)$ BTU/hr.ft.^{o}F.

The calculated thermal conductivities demonstrate the highly desirable characteristic of the heat pipe operation

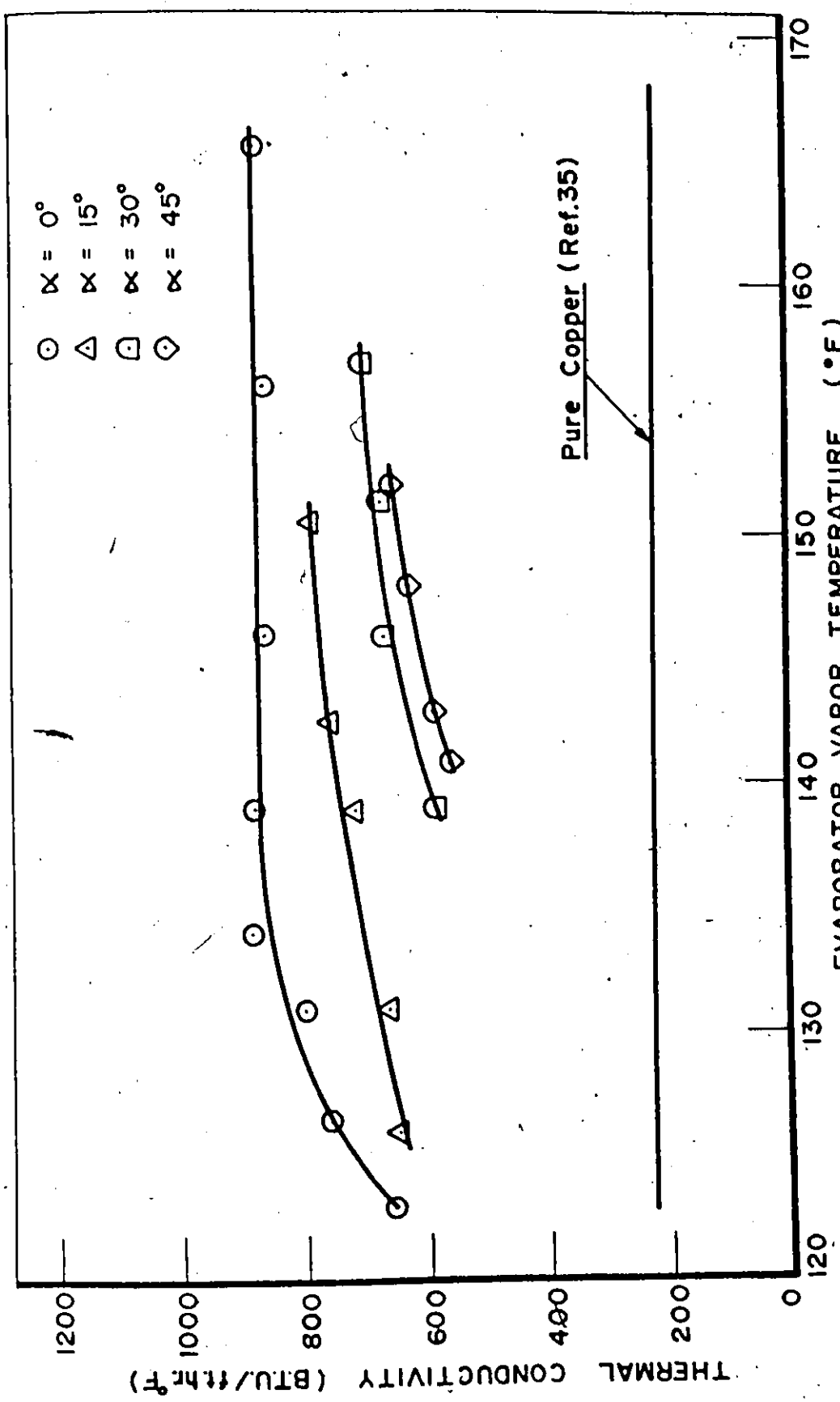

Fig.19 Equivalent Thermal Conductivity versus Vapor Temperature

which is high heat transfer rates with low temperature gradients. Taking as an example the heat pipe in the horizontal direction at a power input of 150 watts, the effective thermal conductivity of the pipe is 890.6 BTU/hr. ft.^{o}F which is four times greater than the conductivity of pure copper. If the equivalent thermal conductivity is based on the temperature drop between the average temperatures in the evaporator and the condenser respectively ($\Delta T = 70^{o}F$; Figure 13) a value of 1370 BTU/hr.ft.^{o}F is obtained. This is compared to 2521 BTU/hr.ft.^{o}F if the theoretical temperature drop is used. The equivalent thermal resistance equal to ($\Delta X/k$) and based on average temperatures in the evaporator and condenser is 5.7×10^{-4} ft^{2}.hr.^{o}F/BTU.

By examining Figure 19, the effective thermal conductivity is proportional to the evaporator vapor temperature, which in turn is proportional to the heat flux (Figure 17), meaning that the rate of increase of the heat transferred is higher than that of the associated temperature drop. As the maximum heat transfer is approached, the curves show a tendency to flatten. This tendency is very clear for the $\alpha = 0$ curve where the thermal conductivity becomes approximately constant for vapor temperatures higher than 140^{o}F. The equivalent thermal conductivity is inversely proportional to the inclination of the heat pipe due to the higher temperature drops.

b. Specific Output

A comparison has been made to determine the amount of heat transferred per unit of weight, for the heat pipe

and a solid copper rod of the same shape.

The weight of the streamlined heat pipe under investigation is 0.5 lbs. The heat transferred per unit weight of the heat pipe is tabulated in Appendix D, and plotted in Figure 20 against the operating temperature.

The values of the specific output calculated are compared on the same plot, with those obtained if the heat pipe was to be replaced by a solid pure copper rod having the same volume as the heat pipe and the same temperature drop applied at each power level.

The volume of the heat pipe was 3.188×10^{-3} ft^3 giving an equivalent copper rod of 1.78 lbs. Applying Fourier's conduction equation to the equivalent copper rod, the heat transferred per unit weight was equal to $0.184\ \Delta T_p$, where ΔT_p is the temperature drop along the heat pipe in ^{o}F.

An inspection of the data obtained, shows another desirable property of the heat pipe, which is its relatively high specific output when compared to solid conductors. For example, in the horizontal direction at a heat input of 150 watts, the heat transferred per unit weight of the heat pipe is 285.3 watts/lb_m compared to 19.7 watts/lb_m for the equivalent copper rod. It should also be noticed from the plot (Figure 20) that the rate of increase of the specific output for the heat pipe as a function of the operating temperature is much higher than that for the solid copper rod.

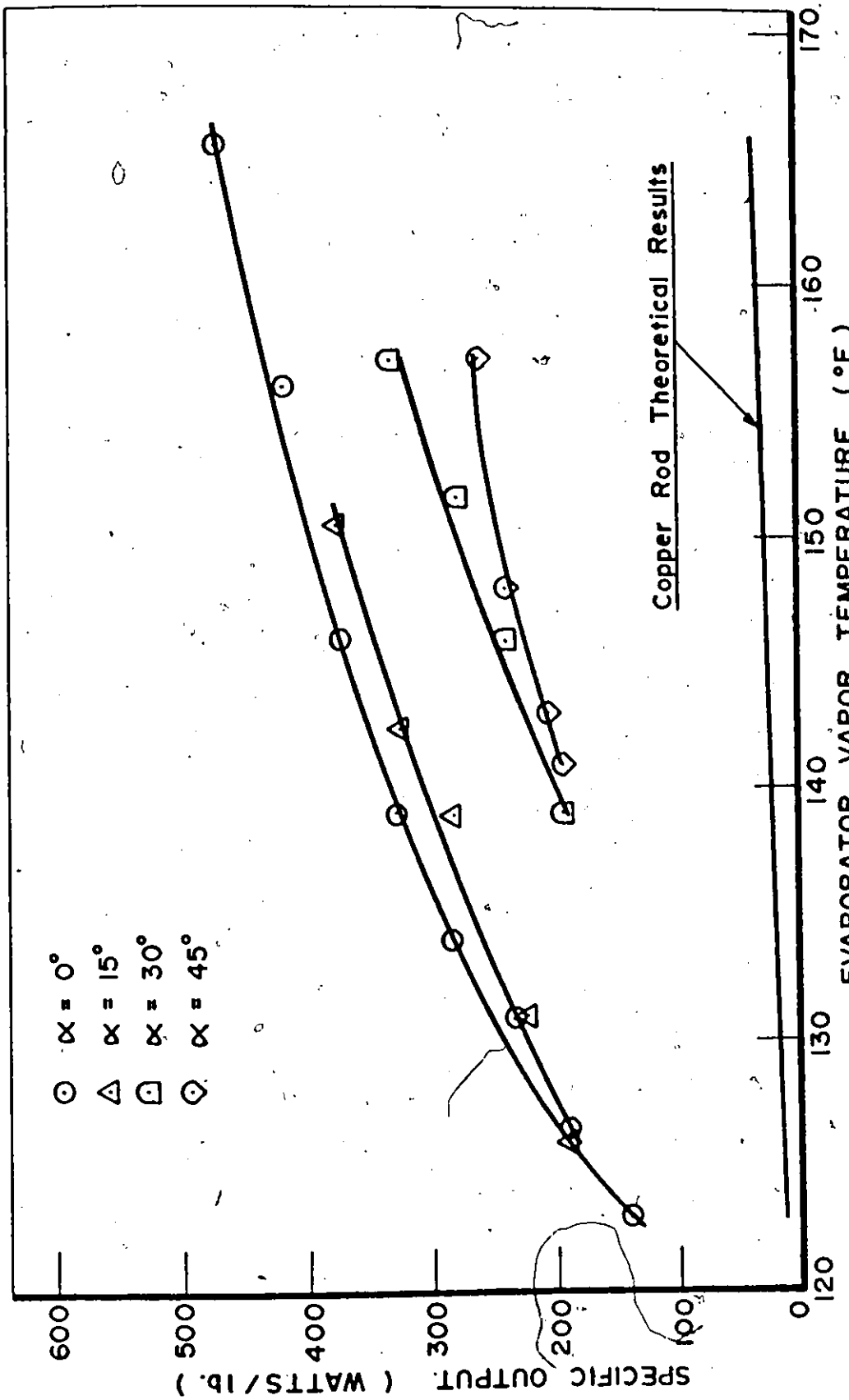

Fig. 20 Specific Output versus Vapor Temperature

CHAPTER V

CONCLUSIONS AND RECOMMENDATIONS

The investigation presented the performance of a new shape of heat pipe: a streamlined cross-section heat pipe. The working fluid used was water and the wick consisted of layers of 200 mesh stainless steel screen. The axial temperature distributions, performance data and parameters, at various power input and angles of inclination have been presented, analysed and compared with existing theories and previous investigations.

The following conclusions and recommendations can be drawn:

1. The vapor temperature difference between the evaporator and the condenser was minimum, thus indicating successful operation of the heat pipe.
2. The axial temperature distributions obtained agreed reasonably well with theory and previous experiments.
3. The vapor temperature and temperature drop along the heat pipe were proportional to the heat input and inclination of the pipe.
4. The heat pipe transferred a maximum heat of 250 watts while installed horizontally. As the evaporator was raised above the condenser the maximum heat decreased. The variation of the maximum heat transfer with inclination was found to be represented by the theoretical model

given by McKinney (23) if the wick permeability is 2×10^{-10} ft^2. and the product $(\sigma \cos\theta_c)$ is approximately 9×10^{-3} lb_f/ft.

5. The power limitations of the heat pipe were due to a capillary pumping limitation. This means that prior to designing a heat pipe, one should obtain all the pertinent information about the wick (permeability, pore size, capillary height and contact angle) by experimental means if they are not found in the published literature or if the validities of the published figures are in doubt. An estimation of these values is of little use in designing a heat pipe for maximum efficiency of heat transfer.

6. The contribution of axial heat conduction was seen to be negligible as compared to the total heat output.

7. Great care has to be taken in the manufacture, cleaning, sealing and filling of the heat pipe if it is to operate properly.

8. If at all possible, the heat pipe should be designed so that visual observations can be made of the interior of the pipe during operation (everted heat pipe). This is of particular interest for observation of the fundamental phenomena involved in the operation of a heat pipe.

9. If a screen wick has to be used for a streamlined cross-section heat pipe, methods should be developed to ensure smooth installation of the wick, and uniform

contact between the wick and the pipe wall. If not, other wicks should be investigated such as textile fabrics or beads packed in an annulus between a retaining screen and the pipe wall.

10. The experiments also demonstrated the highly desirable characteristics of heat pipes, which are high equivalent thermal conductivities and specific outputs.

11. The present streamlined heat pipe was designed primarily for an air-to-air heat exchanger. Consequently, future study may consist of testing the streamlined heat pipe under aerodynamic conditions, in which the addition and rejection of heat are effected by flow phenomenon around the body.

APPENDIX A

OPTIMIZATION STUDY

A.1. Introduction

It had been suggested that cooling air might be supplied to the compressor impeller backface of an up-rated jet engine to alleviate an apparently unacceptable stress-temperature situation. As a possible solution to the problem it was proposed that a certain amount of compressor bleed air be cooled in a heat exchanger located in the annular by-pass duct. The cooled air was then to be ducted to the impeller backface cavity.

The operating conditions for the heat exchanger and typical dimensions are shown schematically in Figure 21.

A.2. Conduction Approach to the Study

As a first approach to the study, it was suggested that the heat load could be exchanged from the hot bleed air to the cold by-pass air, by means of installing a number of solid rod conductors at the insulating interface between both streams in the circumferential and the axial directions respectively.

The mechanism of heat transfer would be by convection from the hot air to the solid rods (L_h), then by conduction along each solid rod, and finally by convection

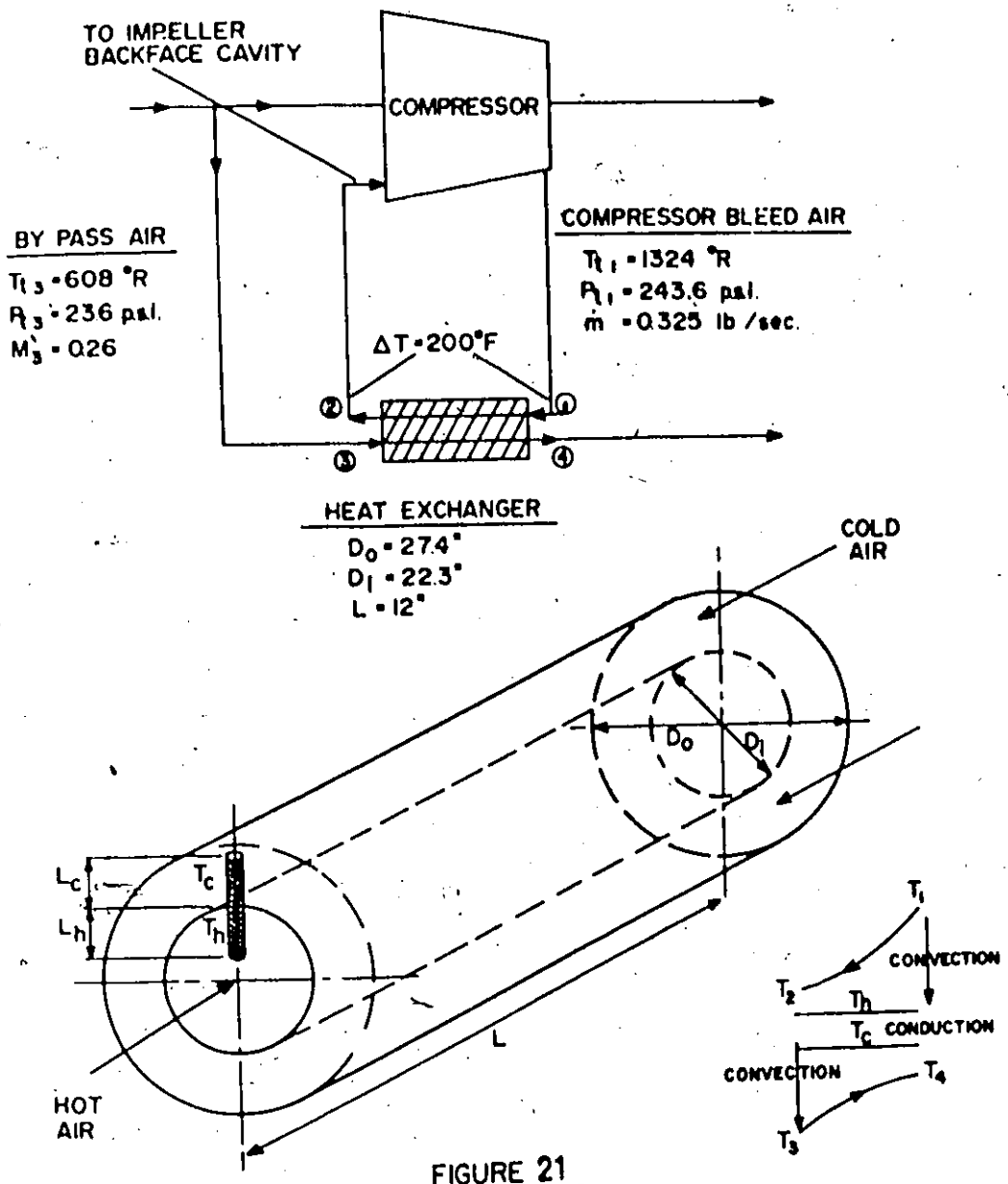

FIGURE 21

BLEED AIR HEAT EXCHANGER CONFIGURATION

from the solid rods (L_c) to the cold air (Figure 21).

A.3. Optimization Formulation

The aim of the optimization study was to determine the minimum number of solid conductors (M x N) capable of transferring the heat load from the hot to the cold stream.

After formulating the problem (Reference 36), twelve runs of the optimization subroutine SEEK 3 (Reference 37) were carried out with four limitations on the thermal resistance R (10^{-6}, 10^{-5}, 10^{-4} and 10^{-3} ft^2 hr $^{o}R/BTU$) and three limitations on the length of the solid rod in the hot stream L_h (4, 5 and 6 inches).

A.4. Results

The optimum solutions as obtained from the twelve runs are tabulated in Table I. A two-dimensional plot was prepared showing the variation of the optimum solution MN with R for different L_h (Figure 22). Finally the optimization surface was plotted, using subroutine PLOT 3D (Reference 37), and shown in Figure 23.

A.5. Discussion of Results

From the optimization point of view, the best solutions obtained among all runs were at $R \geq 1 \times 10^{-6}$. This meant that the rod material had to have high thermal conductance, a property which may not be found in any solid

L_h (Inches)	R (ft^2 hr^oR/BTU (greater than)	MN	R (ft^2 hr^oR/BTU)	D (Inches)	T_c (^oR)	T_h (^oR)	L_c (Inches)	L_h (Inches)
4	1×10^{-6}	85.9	1.26×10^{-6}	1.0	662.5	662.7	2.49	4.0
	1×10^{-5}	86.1	1.01×10^{-5}	1.0	662.4	663.7	2.49	4.0
	1×10^{-4}	87.7	1×10^{-4}	1.0	661.4	673.9	2.49	4.0
	1×10^{-3}	104.0	1×10^{-3}	1.0	652.4	758.2	2.49	4.0
5	1×10^{-6}	70.4	2.82×10^{-6}	1.0	675.4	675.9	2.49	5.0
	1×10^{-5}	70.5	1.08×10^{-5}	1.0	675.3	677.0	2.49	5.0
	1×10^{-4}	72.2	1×10^{-4}	1.0	673.7	688.9	2.49	5.0
	1×10^{-3}	88.5	1×10^{-3}	1.0	660.8	785.0	2.49	5.0
6	1×10^{-6}	60.1	5.68×10^{-6}	1.0	687.6	688.7	2.49	6.0
	1×10^{-5}	60.2	1.27×10^{-5}	1.0	687.5	689.8	2.49	6.0
	1×10^{-4}	61.8	1×10^{-4}	1.0	685.3	703.4	2.49	6.0
	1×10^{-3}	78.2	1×10^{-3}	1.0	668.3	809.3	2.49	6.0

TABLE I. Optimization Study Results

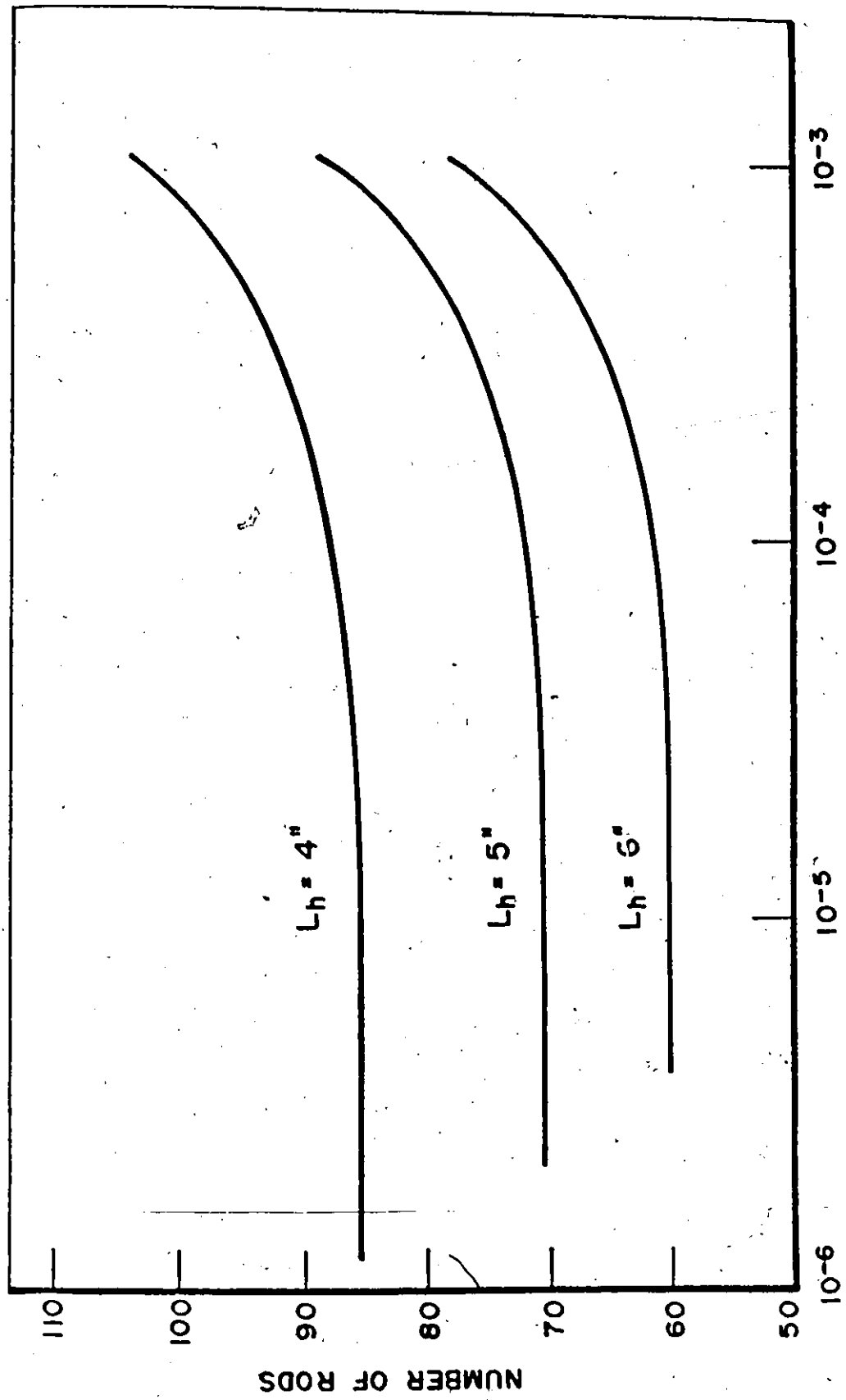

Fig.22 Variation of Rod Number with Thermal Resistance

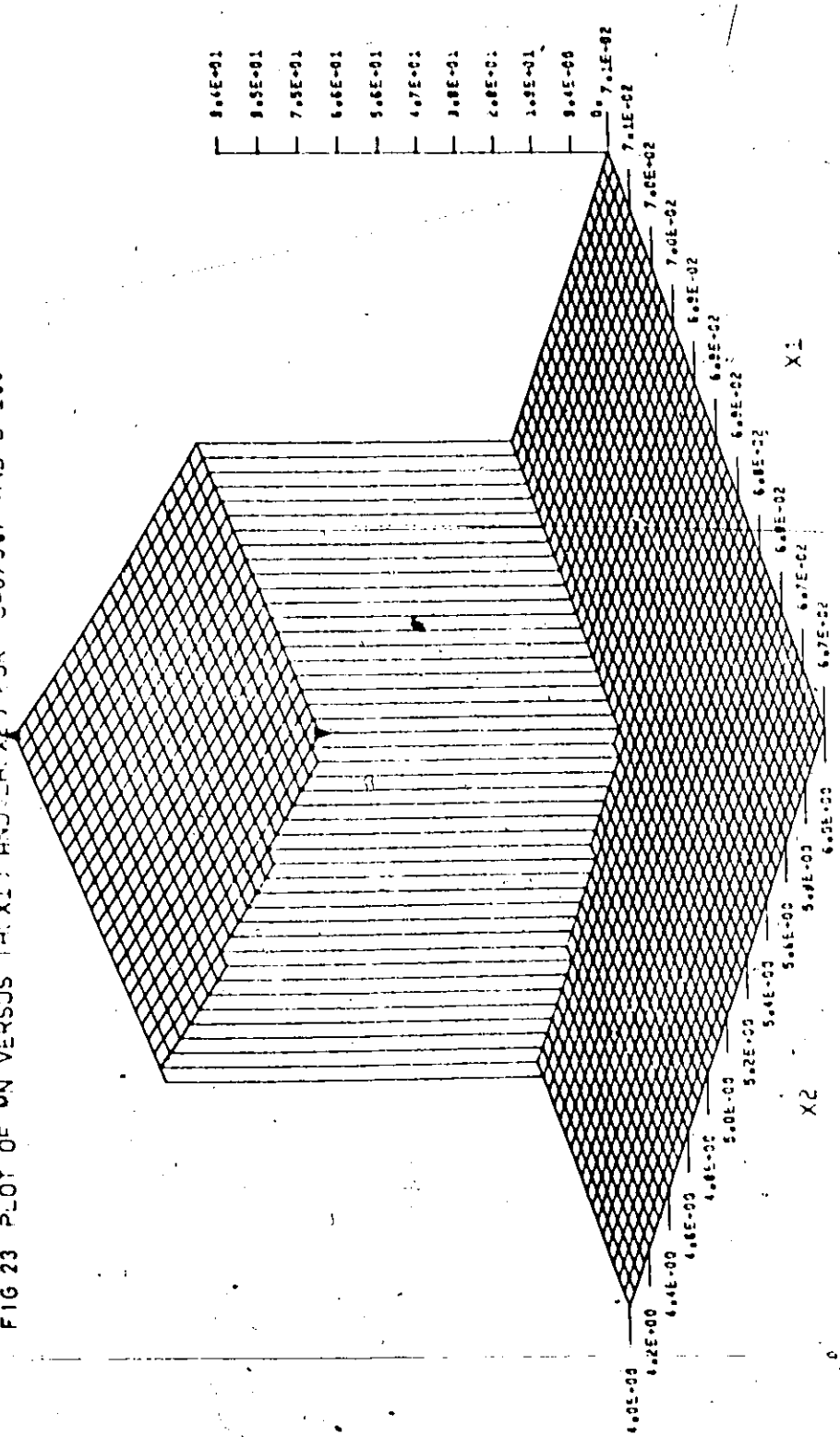

FIG 23 PLOT OF WN VERSUS TH(X1) AND(H(X2) FOR TC=673.7 AND D=1.0

conductor. It was also seen that if the thermal resistance was increased to 1×10^{-5} and even to 1×10^{-4} the optimum number of rods did not increase appreciably, so that these solutions were more preferable from the heat transfer point of view. Finally the solutions for $R \geq 1 \times 10^{-3}$ were rejected as they led to a comparatively high number of rods.

Taking the optimum solution of all runs with a value of $R \geq 1 \times 10^{4}$, it was found that MN was equal to 62, 72 and 88 at an L_h equal to 6, 5 and 4 inches respectively. This gave a heat load per conductor equal to 300, 240 and 200 watts respectively.

A.6. Conclusion

This primary study enabled us to predict the optimum number, main dimensions, temperatures and thermal resistances of one of the methods of heat exchange, i.e., solid rod conductors. But we see that the required thermal conductance was very high so that an actual solution to the problem could not be achieved using solid conductors. However, a solution to the problem of high conductance may be found by substituting for the solid conductor a recent development in the field of thermodynamics termed a "heat pipe".

APPENDIX B

ESTIMATION OF WICK THICKNESS

The heat pipe theory developed up to date was due, in a large part, to a stimulus provided in a theoretical study performed by Cotter (2). He formulated the governing equations describing the processes taking place in a heat pipe and also developed a model to predict the capillary limit of heat pipe operation. His results were used by McKinney (23) who simplified and modified the equations to get the maximum heat transfer by cylindrical heat pipe, at capillary limiting conditions, as a function of pipe geometry, fluid properties, and wick properties and dimensions. The modified equation (23) may be written as follows,

$$Q_{max} = \left(\frac{2\sigma\cos\theta_c}{r} - \rho_\ell \frac{g}{g'} L_p \cos\beta\right)\left[\frac{r_2^2(\zeta^4 - \zeta^6)}{B\, r_2^2(1-\zeta^2) + C\, r_2^4\, \zeta^4}\right] \qquad (B.1)$$

where,

$$\zeta = \left(\frac{r}{r_2}\right)$$

$$B = \frac{4\,\mu_v\,(L_p + L_a)}{\pi\,\rho_v\,\lambda}$$

$$C = \frac{\mu_\ell\,(L_p + L_a)}{2\pi K \rho_\ell\,\lambda}$$

Figure 24 describes the geometry of the heat pipe.

By examining Equation (B.1), one sees that the maximum heat transfer by a heat pipe depends on several factors.

First is the fluid vapor temperature or operating temperature T_v, which determines the liquid and vapor density and viscosity (ρ_ℓ, ρ_v, μ_ℓ and μ_v), the latent heat of vaporization (λ), the surface tension (σ), and the apparent contact angle (θ_e). The second factor concerns the wick characteristics defined by the permeability (K), the pore radius (ε) and the wick thickness (r_3/r_2). Finally one introduces the heat pipe dimensions (L_p, L_a, and r_2), and orientation (β).

Treating the streamlined heat pipe as a circular one having the same cross-section area, a computer program was prepared to calculate the maximum heat transfer (Q_{max}) as a function of wick thickness (r_3/r_2) for various operating temperatures (T_v = 100, 150, 200, 250 and 300°F). The heat pipe was assumed to be horizontally installed, the working fluid being water and the wick 200 mesh of 304 stainless steel wire with a diameter of 0.0021 inch.

Table II presents the property values of water for computer input as a function of the selected operating temperatures T_v. The values were taken from References 33, 39 and 40. The heat pipe dimensions and characteristics were as follows,

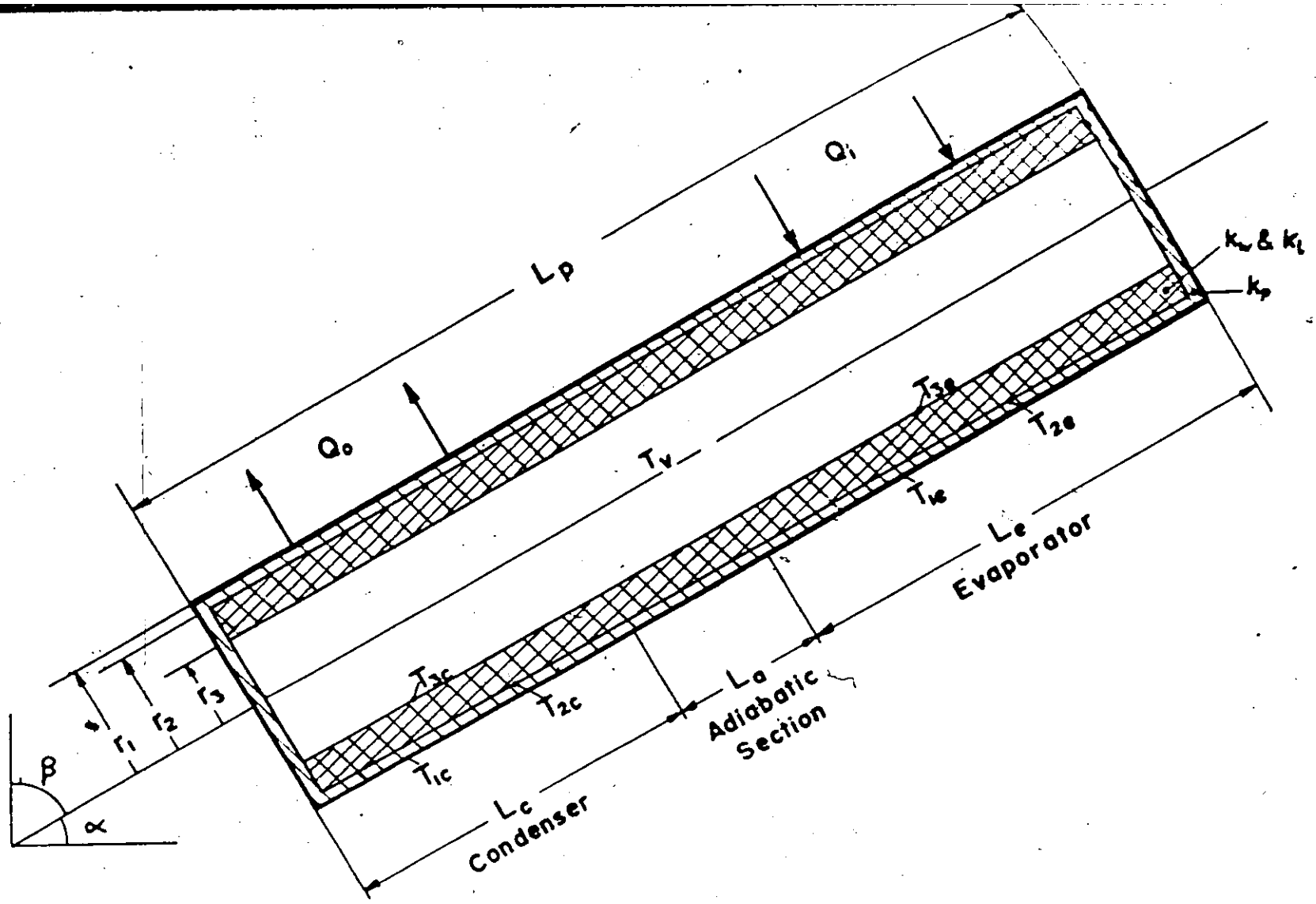

Fig.24 Schematic Drawing of a Heat Pipe showing both the Temperature and Geometry Notation

Temperature		100°F	150°F	200°F	250°F	300°F
σ	lb_f/ft	4.78×10^{-3}	4.45×10^{-3}	4.1×10^{-3}	3.75×10^{-3}	3.4×10^{-3}
ρ_ℓ	lb_m/ft^3	62	61.1	60.1	58.8	57.3
ρ_v	lb_m/ft^3	2.85×10^{-3}	1.03×10^{-2}	3×10^{-2}	7.2×10^{-2}	1.55×10^{-1}
μ_ℓ	$lb_f hr/ft^2$	4×10^{-9}	2.53×10^{-9}	1.77×10^{-9}	1.32×10^{-9}	1.05×10^{-9}
μ_v	$lb_f hr/ft^2$	5.22×10^{-11}	6.4×10^{-11}	7.3×10^{-11}	8.0×10^{-11}	8.6×10^{-11}
λ	BTU/lbm	1037.2	1007.2	977.9	945.5	910.1

TABLE II Properties for Computer Input

$L_p = 0.78$ ft

$L_a = 0.073$ ft

$r_1 = 0.43$ inch

$r_2 = 0.401$ inch

$$\varepsilon = \frac{1 - \text{Mesh size} \times \text{Wire diameter}}{\text{Mesh size}} \quad (23)$$

$$= 2.41 \times 10^{-4} \text{ ft}$$

Normally the permeability of the wick and the apparent contact angle should be determined experimentally. Reference 24 presented an experimental value for the permeability of 200- mesh 304 stainless-steel screen equal to 3.09×10^{-9} ft^2. This value was used for the present calculations. No data were found for the contact angle and it was assumed equal to zero.

The computer results are tabulated in Table III, and plotted in Figure 25.

By examining Figure 25, for each operating temperature T_v, a maximum heat transfer occured at an optimum value of r_3/r_2. The optimum value of r_3/r_2 was inversely proportional to T_v. From this study, the optimum value of wick thickness should be such that r_3/r_2 would be in the range 0.3 to 0.5. However for the experiments included here,

r_3/r_2 \ T_v °F	100°F	150°F	200°F	250°F	300°F
0.1	75.1	197.5	440.1	823.0	1365.3
0.2	963.9	2164.3	3877.2	5683.8	7180.5
0.3	2548.3	4459.5	6379.0	7935.2	8862.2
0.4	3321.4	5091.0	6691.1	7936.9	8604.3
0.5	3323.9	4845.8	6195.2	7244.9	7788.1
0.6	2957.7	4229.9	5353.8	6229.5	6677.0
0.7	2397.7	3401.8	4288.0	4979.3	5330.6
0.8	1705.6	2411.0	3035.7	3519.6	3766.0
0.9	903.5	1275.0	1602.8	1858.8	1988.3

TABLE III. Maximum Heat Transfer in Watts as a Function of Operating Temperature and Wick Thickness

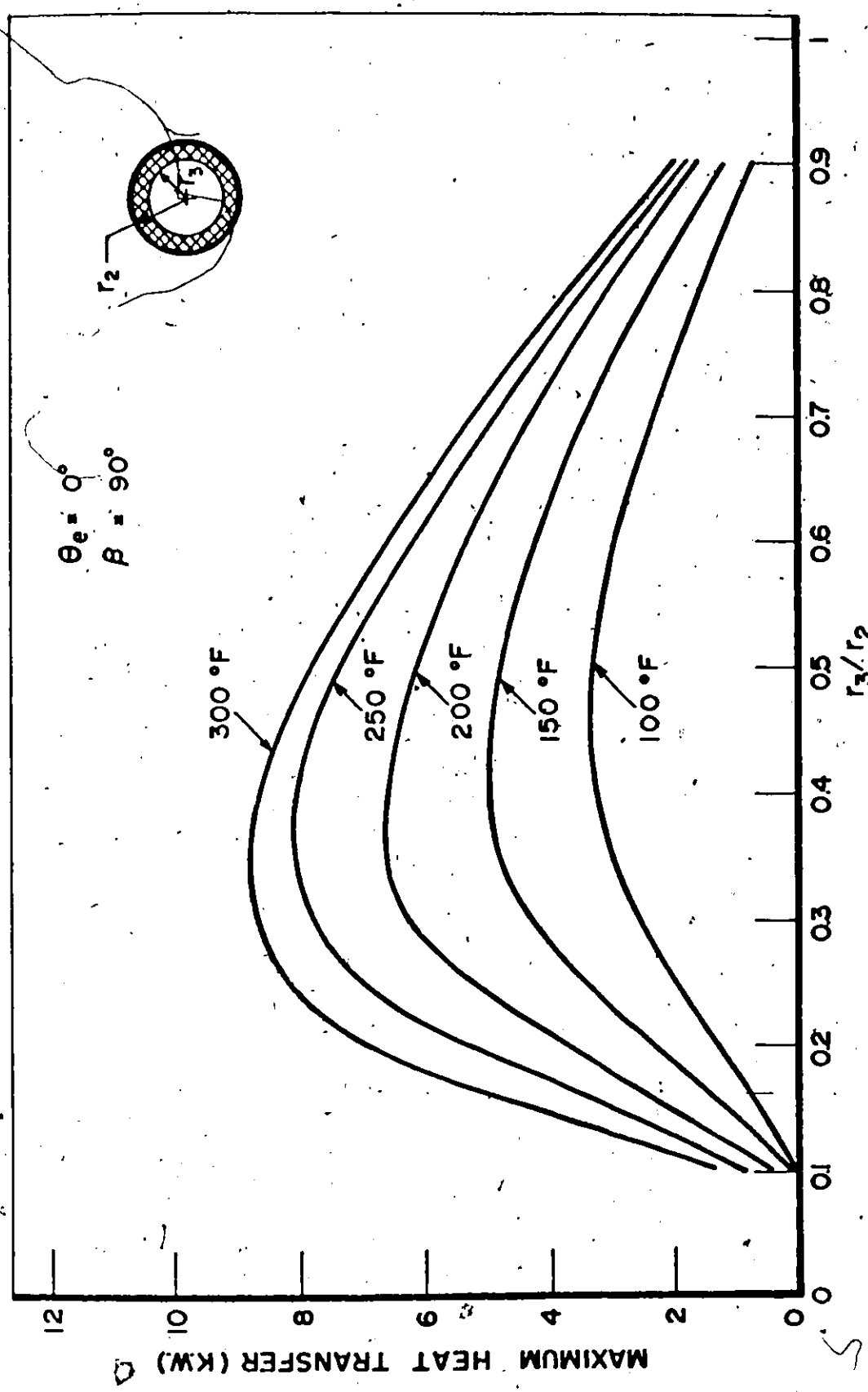

Fig. 25 Maximum Heat Transfer Rates versus r_3/r_2 at various Operating Temperatures

it was decided to limit the wick thickness so that r_3/r_2 would be between 0.8 and 0.9. The factors which determined this range for r_3/r_2 were the results obtained from the optimization study (Appendix A) and the quantity of wicking material available. Also, an additional reason for this selection was to facilitate the installation of the wick into the heat pipe.

APPENDIX C

ASSEMBLY PROCEDURE FOR THE HEAT PIPE PERFORMANCE TEST SYSTEM

The procedure for assembling the heat pipe performance test system was as follows:

1. The pipe inside and outside surfaces were finished with fine grade emery paper.
2. The pipe was washed several times with a dilute solution of hydrochloric acid and then with distilled water.
3. The pipe was degreased using acetone, then washed with distilled water.
4. The water calorimeter and the end cap were silver soldered to the condenser section of the heat pipe.
5. The vacuum fill system was installed at the condenser side, except for the compound pressure gauge which was mounted later after completion of the leak and pressure testing.
6. After preparing and rolling the screen, it was inserted with care into the pipe from the evaporator end.
7. The evaporator end cap was argon welded, and a steady flow of argon was passed through the pipe to reduce the contamination of the inner surface by air.
8. The two vapor core ceramocouples were installed.

9. The pipe was argon pressure and leak tested up to a pressure of 170 p.s.i.g. and down to 1 mm Hg.
10. Some initial leaks were observed and they were treated with epoxy cement to produce an air tight system.
11. The thermocouples measuring the axial temperature distributions in the evaporator and adiabatic sections were spot welded to the heat pipe surface.
12. The heater block parts were clamped tightly to the evaporator outer surface of the heat pipe to provide a good thermal interface (low contact resistance).
13. The four cartridge heaters were installed in the heater block.
14. The pipe was evacuated to a pressure of 1 mm vacuum using an auxiliary mercury column for measurement purposes.
15. The assembly was rotated in a vertical position (evaporator down), and the pipe was loaded by a syringe with 24.0 c.c. of distilled water. Rust inhibitor was also added to the water in the form of sodium dichromate crystals.
16. The pipe was shaken and turned around in all directions to ensure that the screen mesh was completely saturated with water.
17. The condenser ceramocouples were installed (4 in number).
18. The thermocouples were connected to the hot junction terminal strips, and all connections were checked.

19. The evaporator insulation and hoses between the main, thermometer wells, calorimeter and rotameter were installed.

20. The adiabatic section, thermometer wells and hose connections to the calorimeter were insulated with fibreglass.

APPENDIX D

HEAT PIPE PERFORMANCE DATA

Tables IV through VII present the performance data obtained for the streamlined heat pipe at the four different orientations, $\alpha = 0^{\circ}$, 15°, 30° and 45° where α is the inclination of the pipe with the horizontal (condenser down).

Power Input (Watts)	75	100	125	150
Water Flow Rate (c.c./min.)	280	325	325	325
Water Inlet Temperature (^{o}C)	20.0	18.7	17.5	16.3
Water Outlet Temperature (^{o}C)	23.5	22.8	22.5	22.5
Power Output (Watts)	69.38	94.34	115.05	142.66
Efficiency (%)	92.51	94.34	92.04	95.1
Condenser Vapor Temperature (^{o}F)	121.0	126.0	131.0	134.0
Condenser Vapor Pressure (in Hg)	3.5	4.0	4.5	5.0
Pressure (Steam Table) (inch)	3.3	4.06	4.64	5.03
Vapor Temperature Drop (^{o}F)	2.0	0.5	0.0	0.0
Adiabatic Section Temperature Drop (^{o}F)	45.75	54.5	61.15	68.7
Axial Heat Conduction (Watts)	2.16	2.56	2.88	3.23
Axial Heat Conduction Percentage (%)	3.11	2.71	2.50	2.26
Heat Pipe Temperature Drop (^{o}F)	70.6	82.45	96.3	107.6
Equivalent Thermal Conductivity (BTU/hr.ft.^{o}F)	659.4	767.8	801.6	890.6
Power Output per lbs. for Heat Pipe (Watts/lbs.)	138.8	188.7	230.1	285.3
Equivalent Power Output per lbs for Copper Rod (Watts/lb.)	12.97	15.15	17.69	19.74

Table IV Performance Data of the Heat Pipe at $\alpha = 0^{o}$

Power Input (Watts)	175	200	225	250
Water Flow Rate (c.c./min.)	325	360	360	340
Water Inlet Temperature (^{o}C)	15.5	14.8	15.0	15.0
Water Outlet Temperature (^{o}C)	22.6	22.1	23.2	24.5
Power Output (Watts)	163.37	186.06	209	235.41
Efficiency (%)	93.35	93.03	92.89	94.16
Condenser Vapor Temperature (^{o}F)	139.0	146.0	156.0	165.5
Condenser Vapor Pressure (in Hg)	5.5	6.5	8.0	10.0
Pressure (Steam Table) (inch)	5.73	6.85	8.76	10.9
Vapor Temperature Drop (^{o}F)	0.0	0.0	0.0	0.0
Adiabatic Section Temperature Drop (^{o}F)	77.25	91.6	113.2	119.05
Axial Heat Conduction (Watts)	3.64	4.32	5.34	5.61
Axial Heat Conduction Percentage (%)	2.22	2.32	2.55	2.38
Heat Pipe Temperature Drop (^{o}F)	123.9	144.2	162.7	179.6
Equivalent Thermal Conductivity (BTU/hr.ft.^{o}F)	884.7	865.8	861.9	879.5
Power Output per lbs. for Heat Pipe (Watts/lbs.)	326.7	372.1	418.0	470.8
Equivalent Power Output per lbs for Copper Rod (Watts/lb.)	22.77	26.50	29.90	33.01

Power Input (Watts)	100	125	150	175	200
Water Flow Rate (c.c./min.)	500	500	500	500	500
Water Inlet Temperature (^{o}C)	17.3	16.4	16.3	16.1	16.7
Water Outlet Temperature (^{o}C)	20.0	19.6	20.3	20.7	22.0
Power Output (Watts)	95.58	113.28	141.60	162.84	187.63
Efficiency (%)	95.58	90.62	94.40	93.05	93.81
Condenser Vapor Temperature (^{o}F)	123.5	129.0	137.0	141.0	149.0
Condenser Vapor Pressure (in Hg)	4.5	5.0	5.5	6.5	7.5
Pressure (Steam Table) (inch)	3.74	4.4	5.4	6.03	7.38
Vapor Temperature Drop (^{o}F)	2.5	2.0	2.0	1.5	1.5
Adiabatic Section Temperature Drop (^{o}F)	69.9	74.4	81.5	92.4	108.0
Axial Heat Conduction (Watts)	3.29	3.50	3.83	4.35	5.09
Axial Heat Conduction Percentage (%)	3.44	3.08	2.70	2.67	2.71
Heat Pipe Temperature Drop (^{o}F)	98.3	114.4	131.0	143.5	158.7
Equivalent Thermal Conductivity (BTU/hr.ft.^{o}F)	652.4	664.4	725.3	761.4	793.3
Power Output per lbs. for Heat Pipe (Watts/lbs.)	191.2	226.6	283.2	325.7	375.3
Equivalent Power Output per lbs for Copper Rod (Watts/lb.)	18.06	21.02	24.07	26.37	29.16

Table V Performance Data of the Heat Pipe at $\alpha = 15^{o}$

Power Input (Watts)	100	130	150	175
Water Flow Rate (c.c./min.)	325	325	325	325
Water Inlet Temperature (^{o}C)	20.8	19.8	19.0	18.8
Wator Outlet Temperature (^{o}C)	25.0	25.0	25.0	26.0
Power Output (Watts)	96.64	119.65	138.06	165.67
Efficiency (%)	96.64	92.04	92.04	94.67
Condenser Vapor Temperature (^{o}F)	136.5	143.0	148.0	154.5
Condenser Vapor Pressure (in Hg)	6.0	6.5	7.5	8.0
Prossure (Steam Table) (inch)	5.35	6.35	7.2	8.4
Vapor Temperature Drop (^{o}F)	2.5	3.0	3.5	2.5
Adiabatic Section Temperature Drop (^{o}F)	57.1	67.4	71.2	74.5
Axial Heat Conduction (Watts)	2.68	3.17	3.30	3.51
Axial Heat Conduction Percentage (%)	2.77	2.65	2.39	2.12
Heat Pipe Temperature Drop (^{o}F)	110.1	120.2	137.4	157.55
Equivalent Thermal Conductivity (BTU/hr.ft.^{o}F)	588.9	667.9	674.2	705.6
Power Output per lbs. for Heat Pipe (Watts/lbs.)	193.3	239.3	276.1	331.3
Equivalent Power Output per lbs for Copper Rod (Watts/lb.)	20.23	22.09	25.25	28.95

Table VI Performance Data of the Heat Pipe at $\alpha = 30^{o}$

Power Input (Watts)	100	110	125	140
Water Flow Rate (c.c./min.)	325	325	325	300
Water Inlet Temperature (^{o}C)	20.0	20.0	20.0	20.0
Water Outlet Temperature (^{o}C)	24.2	24.4	25.2	26.2
Power Output (Watts)	96.64	101.25	119.65	131.68
Efficiency (%)	96.64	92.03	95.72	94.06
Condenser Vapor Temperature (^{o}F)	134.0	138.0	144.0	148.5
Condenser Vapor Pressure (in Hg)	6.0	6.5	7.5	8.0
Prossure (Steam Table) (inch)	5.03	5.58	6.5	7.2
Vapor Temperature Drop (^{o}F)	7.0	5.0	4.0	3.5
Adiabatic Section Temperature Drop (^{o}F)	58.0	60.5	65.5	68.2
Axial Heat Conduction (Watts)	2.73	2.85	3.08	3.20
Axial Heat Conduction Percentage (%)	2.82	2.81	2.57	2.43
Heat Pipe Temperature Drop (^{o}F)	115.45	114.8	127.75	134.25
Equivalent Thermal Conductivity (BTU/hr.ft.^{o}F)	561.7	591.8	628.4	658.2
Power Output per lbs. for Heat Pipe (Watts/lbs.)	193.3	202.5	239.3	263.4
Equivalent Power Output per lbs for Copper Rod (Watts/lb.)	21.21	21.18	23.48	24.67

Table VII Performance Data of the Heat Pipe at $\alpha = 45^{o}$

APPENDIX E

CALCULATION OF THEORETICAL TEMPERATURE DISTRIBUTION ALONG THE HEAT PIPE

In order to compare the experimental temperature distribution with theory, Appendix E presents calculation of the theoretical temperature drops along a cylindrical heat pipe. The present streamlined heat pipe is treated as a circular one having the same cross-section area, taking as an example the heat pipe installed in the horizontal direction at a power input of 150 watts.

Figure 24 in Appendix B shows the main heat flow paths and temperature drops across a heat pipe. The temperature drop between the heat pipe surface and the vapor can be divided into two parts. Taking the evaporator as an example, the first temperature drop is $(T_{1e}-T_{3e})$ and the second $(T_{3e}-T_v)$.

The temperature drop $(T_{1e}-T_{3e})$ across the pipe wall and the liquid-wick matrix is due to conduction. Heat transfer by convection in the liquid-wick matrix has been neglected, as the pores are too small for any significant convection currents to develop. For the evaporator section one may write

$$T_{1e}-T_{2e} = \frac{Q_i}{2\pi L_e k_p} \ln \left(\frac{r_1}{r_2}\right)$$

and

$$T_{2e}-T_{3e} = \frac{Q_i}{2\pi L_e k_{\ell w}} \ln \left(\frac{r_2}{r_3}\right)$$

Combining the two equations one obtains for the evaporator section,

$$T_{1e}-T_{3e} = \frac{Q_i}{2\pi L_e}\left[\frac{1}{k_p}\ln\frac{r_1}{r_2} + \frac{1}{k_{\ell w}}\ln\frac{r_2}{r_3}\right] \qquad (E.1)$$

Here the effective thermal conductivity of the liquid-wick matrix $k_{\ell w}$, assumed constant, may be calculated by assuming that the liquid and the wick material present parallel paths for heat flow. In this case, the total heat transfer rate is the sum of the heat transfer rates through the two paths. In a finite difference form this can be written

$$Q_{total} = k_\ell A_\ell \frac{\Delta T}{\Delta X} + k_w A_w \frac{\Delta T}{\Delta X}$$

Dividing both sides by A, the total heat transfer area, gives

$$\frac{Q}{A} = k_\ell \phi \frac{\Delta T}{\Delta X} + k_w (1-\phi) \frac{\Delta T}{\Delta X}$$

hence $k_{\ell w} = k_\ell \phi + k_w (1-\phi)$

The temperature drop $(T_{3e}-T_v)$ can be calculated by applying the Clausius-Clapeyron equation (11) written in a finite difference form,

$$\frac{\Delta P}{T_{3e}-T_v} = \frac{\lambda \rho_v}{T_v}$$

where ΔP is the capillary pressure difference (11),

$$\Delta P = \frac{2\sigma}{\varepsilon\phi}\cos\theta_e$$

Combining the two equations one obtains for the evaporator section,

$$T_{3e}-T_v = \frac{2\sigma}{\phi\varepsilon}\ \frac{T_v}{\lambda\rho_v}\ \cos\theta_e \qquad (E.2)$$

Equations (E.1) and (E.2) define the radial temperature drop in the evaporator of a heat pipe. Similar equations can be obtained for the condenser section.

Sample Calculations (Horizontal Orientation; Power = 150 watts)

For the evaporator,

$$T_{1e}-T_{3e} = \frac{Q_i}{2\pi L_e}\ \left[\frac{1}{k_p}\ln\frac{r_1}{r_2} + \frac{1}{k_{\ell w}}\ln\frac{r_2}{r_3}\right]$$

$$T_{3e}-T_v = \frac{2\sigma}{\phi\varepsilon}\ \frac{T_v}{\lambda\rho_v}\ \cos\theta_e$$

From Table 3 in Appendix D at a power input of 150 watts, Q_o = 142.66 watts and T_v = 134°F. Considering all property values to be taken at T_v the following values are obtained:

k_p = 24.67 BTU/hr.ft.°F (34)

k_ℓ = 0.38 BTU/hr.ft.°F (35)

k_w = 8.8 BTU/hr.ft.°F (35)

σ = 4.6 x 10^{-3} lb_f/ft, (40)

λ = 1017.6 BTU/lb_m (33)

ρ_v = 0.007 lb_m/ft^3. (33)

also

L_e = 0.5 ft.

$$\phi = 66.4\% \qquad (38)$$

From Appendix B,

$r_1 = 0.43$ inch

$r_2 = 0.401$ inch

$\varepsilon = 2.41 \times 10^{-4}$ ft.

$\theta_e = 0.0$

From Section 3.4, the wick thickness is given as 0.055 inch. This corresponds to a value of $r_3 = 0.346$ inch $(r_3/r_2 = 0.865)$. Hence $k_{\ell w} = 3.2$ BTU/hr.ft.$^\circ$F

$T_{1e} - T_{3e} = 7.6^\circ$F

$T_{3e} - T_v = 6.16^\circ$F

so $T_{1e} = 147.71^\circ$F

Similarly for the condenser $T_{1c} = 109.74^\circ$F.

REFERENCES

1. G. M. Grover, T. P. Cotter, and G. F. Erickson, "Structures of Very High Thermal Conductance", J. Appl. Phys., Vol. 35, No. 6, June 1964, pp. 1990-1991.

2. T. P. Cotter, "Theory of Heat Pipes", Los Alamos Sci. Lab., LA-3246-MS, Feb. 1965.

3. V. H. Gray, "The Rotating Heat Pipe", Presented at the ASME-AIChE Heat Transfer Conference, Minneapolis, Minn., Aug. 3-6, 1969, Paper No. 69-HT-19.

4. T. B. Jones, "An Electrohydrodynamic Heat Pipe", Presented at the ASME Winter Annual Meeting, New York, Nov. 26-30, 1972, Paper No. 72-WA/HT.35.

5. K. T. Feldman, Jr. and G. H. Whiting, "Applications of the Heat Pipe", Mech. Eng., 48-53 (1968).

6. E. C. Conway and M. J. Kelley, "A Continuous Heat Pipe for Spacecraft Thermal Control", Annual Aviation and Space Conference, California, June 1968, pp. 655-8.

7. E. R. F. Winter and W. D. Barsch, "The Heat Pipe", Advances in Heat Transfer, Vol. 7, Academic Press, New York, 1971, pp. 219-320.

8. T. E. Deverall and J. E. Kemme, "High Thermal Conductance Devices Utilizing the Boiling of Lithium or Silver", Los Alamos Sci. Lab., LA-3211, April 1965.

9. G. H. Parker and J. P. Hanson, "Heat Pipe Analysis", Intersociety Energy Convers. Eng. Conf., Miami Beach, Fla, 847-57 (1967).

10. K. T. Feldman, Jr., "Heat Pipe Design and Analysis", Northrop Corp Lab. NCL 68-11R, Feb. 1968.

11. L. G. Neal, "Analytical and Experimental Study of Heat Pipes", TRW Rpt. 99900-6114-R000, Jan. 1967.

12. S. Frank, "Heat Pipe Design Manual", Martin Nuclear Report MND-3288, Martin Marietta Corp., Baltimore, Maryland, Feb. 1967.

13. EUR, Ispra, Italy, "Liquid Metals for Heat Pipes: Properties, Plots and Data Sheets", Rpt. No. EUR-3653 E., No. N68-14750, Nov. 1967.

14. L. Langston and H. R. Kunz, "Vapor Chamber Fin Studies", NASA 3-7622, 1st, 2nd, 3rd Quart. Rpts.

15. J. E. Deverall, "Capability of Heat Pipes", Presented at Heat Pipe Technology and Manned Space Station Applications Technical Interchange, Huntsville, Alabama, May 1969.

16. C. L. Tien, "Theory of Two-Component Heat Pipes", Presented at the ASME Winter Annual Meeting, Washington, D.C., Nov. 28-Dec. 2, 1971, Paper No. 71-WA/HT-30.

17. C. L. Tien, "Two-Component Heat Pipes, Application to Thermal Design of Spacecraft", Academic Press, N.Y., 1970, pp. 423-436.

18. K. T. Feldman and G. L. Whitlow, "Experiments with a Two-Fluid Heat Pipe", Proceedings of 4th Intersociety Energy Conversion Eng. Conf., Washington, D.C., Sept. 1969.

19. J. K. Ferrell and A. Carnesale, "A Study of the Operating Characteristics of the Heat Pipe", Prog. Rpts. ORO-3411-9, North Carolina State Univ., Rayleigh.

20. E. C. Phillips and J. D. Hindermann, "Determination of Properties of Capillary Media Useful in Heat Pipe Design", Presented at the ASME-AIChE Heat Transfer Conf., Minneapolis, Minnesota, Aug. 3-6, 1969, Paper No. 69-HT-25.

21. J. H. Cosgrove, J. K. Ferrell and A. Carnesale, "Operating Characteristics of Capillary Limited Heat Pipes", Journal of Nuclear Energy, 1967, Vol. 21, pp. 547-558.

22. S. Katzoff, "Heat Pipes and Vapor Chambers for Thermal Control of Spacecraft", AIAA Thermophysics Specialist Conf., AIAA 67-310, April 1967.

23. B. McKinney, "An Experimental and Analytical Study of Water Heat Pipes for Moderate Temperature Ranges", Ph.D Dissertation, Univ. of Alabama, 1969.

24. C. C. Roberts and K. T. Feldman, "Predicting Performance of Heat Pipes with Partially Saturated Wicks", Presented at the ASME Winter Annual Meeting, New York, Nov. 26-30, 1972, Paper No. 72-WA/HT-38.

25. J. Bohdansky, "The Use of a New Heat Removal System in Space Thermionic Power Supplies", EUR 2229.3, 1965.

26. J. E. Kemme, "Ultimate Heat Pipe Performance", IEEE Thermionic Conversion Specialist Conf., Framingham, Mass., Oct. 21-23, 1968, pp. 266-71.

27. G. D. Johnson and E. W. Saaski, "Arterial Wick Heat Pipes", Presented at the ASME Winter Annual Meeting, New York, Nov. 26-30, 1972, Paper No. 72-WA/HT-36.

28. W. A. Ranken and J. E. Kemme, "Survey of Los Alamos and Euratom Heat Pipe Investigations", IEEE THermionic Conversion Specialist Conf., San Diego, California, Oct. 1965, pp. 325-36.

29. P. J. Marto and W. L. Mosteller, "Effect of Nucleate Boiling on the Operation of Low Temperature Heat Pipes", Presented at the ASME-AIChE Heat Transfer Conference, Minneapolis, Minn., Aug. 3-6, 1969, Paper No. 69-HT-24.

30. R. Moss and A. Kelly, "Neutron Radiographic Study of Limiting Planar Heat Pipe Performance", J. of Heat and Mass Transfer, 1970, Vol. 13, pp. 491-502.

31. G. S. Dzakowic, Y. S. Tang and F. G. Arcella, "Experimental Study of Vapor Velocity Limit in a Sodium Heat Pipe", Presented at the ASME-AIChE Heat Transfer Conference, Minneapolis, Minn., Aug. 3-6, 1969, Paper No. 69-HT-21.

32. C. A. Busse, "Theory of the Ultimate Heat Transfer Limit of Cylindrical Heat Pipes", J. of Heat and Mass Transfer, 1973, Vol. 16, pp. 169-186.

33. Keenan, Keyes, Hill and Moore, "Steam Tables: Thermodynamic Properties of Water Including Vapor, Liquid and Solid Phases", John Wiley, 1969.

34. N.R.C. Private Communication with G. E. Mair, Engine Laboratory, No. 2-13-6, January 1974.

35. F. Kreith, "Principles of Heat Transfer", International Textbook Company, Scranton, Pa., 1965.

36. S. H. Moustapha, "Bleed-Air Heat Exchanger Optimization Study", Graduate Course (M.E. 716) Project, Mech. Eng. Dept., McMaster Univ., January 1973.

37. J. N. Siddall, "Analytical Decision-Making in Engineering Design", Prentice Hall, 1972.

38. Greening Donald Ltd., Private Communication, June 1973.

39. E. Eckert and M. Drake, "Analysis of Heat and Mass Transfer", McGraw-Hill Book Company, 1972.

40. H. Grober, S. Erk and U. Grigull, "Fundamentals of Heat Transfer", McGraw-Hill Book Company, 1961.